Elsevier Editorial System(tm) for Tectonophysics
Manuscript Draft

Manuscript Number: TECTO10106R2

Title: New constraints on micro-seismicity and stress state in the western part of the North Anatolian Fault Zone: Observations from a dense seismic array

Article Type: Research Paper

Keywords: micro-seismicity; North Anatolian Fault Zone (NAF); stress tensor inversion; dense seismic array

Corresponding Author: Dr. Selda Altuncu Poyraz, Ph.D

Corresponding Author's Institution: Bogazici Univ.Kandilli Observatory and Earthquake Research

First Author: Selda Altuncu Poyraz, Ph.D

Order of Authors: Selda Altuncu Poyraz, Ph.D; Mustafa Uğur Teoman; Niyazi Türkelli; Metin Kahraman; Didem Cambaz; Ahu Mutlu; Sebastian Rost; Gregory A Houseman; David A Thompson; David Cornwell; Murat Utkucu; Levent Gülen

Abstract: With the aim of extensively investigating the crustal structure beneath the western segment of the North Anatolian Fault Zone where it splays into northern and southern branches, a temporary seismic network (Dense array for North Anatolia-DANA) consisting of 70 stations was deployed in early May 2012 and operated for 18 months in the Sakarya region during the FaultLab experiment. Out of 2437 events contaminated by explosions, we extracted 1371 well located earthquakes. The enhanced station coverage having a nominal station spacing of 7 km, lead to a minimum magnitude calculation of 0.1. Horizontal and vertical location uncertainties within the array do not exceed 0.8 km and 0.9 km, respectively. We observe considerable seismic activity along both branches of the fault where the depth of the seismogenic zone was mostly confined to 15 km. Using our current earthquake catalogue we obtained a b-value of 1. We also mapped the b-value variation with depth and observed a gradual decrease. Furthermore, we determined the source parameters of 41 earthquakes with magnitudes greater than 1.8 using P-wave first motion polarity method. Regional Moment Tensor Inversion method was also applied to earthquakes with magnitudes greater than 3.0. Focal mechanism solutions confirm that Sakarya and its vicinity is stressed by a compressional regime showing a primarily oblique-slip motion character. Stress tensor analysis indicates that the maximum principal stress is aligned in WNW-ESE direction and the tensional axis is aligned in NNE-SSW direction.

05.06.2015

Dear Colleague,

We are sending a research paper as titled **“New constraints on micro-seismicity and stress state in the western part of the North Anatolian Fault Zone: Observations from a dense seismic array”** and prepared by **Selda ALTUNCU POYRAZ, M. Uğur TEOMAN, Niyazi TÜRKELLİ, Metin KAHRAMAN, Didem CAMBAZ, Ahu MUTLU, Sebastian ROST, Gregory A. HOUSEMAN, David A. THOMPSON, David CORNWELL, Murat UTKUCU and Levent GÜLEN** hope to publish in **Tectonophysics.**

Best Regards.

Dr. Selda ALTUNCU POYRAZ
Kandilli Observatory and Earthquake Research Institute (KOERI),
National Earthquake Monitoring Center
Bogazici University, Istanbul, Turkey
e-mail: selda.altuncu@boun.edu.tr

Abstract

With the aim of extensively investigating the crustal structure beneath the western segment of the North Anatolian Fault Zone where it splays into northern and southern branches, a temporary seismic network (Dense array for North Anatolia-DANA) consisting of 70 stations was deployed in early May 2012 and operated for 18 months in the Sakarya region during the FaultLab experiment. Out of 2437 events contaminated by explosions, we extracted 1371 well located earthquakes. The enhanced station coverage having a nominal station spacing of 7 km, lead to a minimum magnitude calculation of 0.1. Horizontal and vertical location uncertainties within the array do not exceed 0.8 km and 0.9 km, respectively. We observe considerable seismic activity along both branches of the fault where the depth of the seismogenic zone was mostly confined to 15 km. Using our current earthquake catalogue we obtained a *b*-value of 1. We also mapped the *b*-value variation with depth and observed a gradual decrease. Furthermore, we determined the source parameters of 41 earthquakes with magnitudes greater than 1.8 using P-wave first motion polarity method. Regional Moment Tensor Inversion method was also applied to earthquakes with magnitudes greater than 3.0. Focal mechanism solutions confirm that Sakarya and its vicinity is stressed by a compressional regime showing a primarily oblique-slip motion character. Stress tensor analysis indicates that the maximum principal stress is aligned in WNW-ESE direction and the tensional axis is aligned in NNE-SSW direction.

Reviewer #1: I am satisfied that the manuscript revisions as well as new supplementary material provided by the authors address all of the concerns that I raised in my review of the original version of this paper. I have a few very minor further suggestions for the revised manuscript.

1. There is a typographical error in the Highlights section. "Disscrimination" should be "Discrimination"
2. On line 194 - stress rate (R) should be stress amplitude ratio (R)
3. Figure 9b should be enlarged for improved legibility

David Eaton
University of Calgary

Answers;

1. Corrected
2. Corrected
3. Figure9b enlarged

Highlights

- High precision location of earthquakes detected by a dense seismic array
- Discrimination of possible quarry blasts and identifying their locations
- *b*-value Analysis
- Determination of focal mechanism solutions and orientations of principal stresses

New constraints on micro-seismicity and stress state in the western part of the North Anatolian Fault Zone: Observations from a dense seismic array

Selda ALTUNCU POYRAZ [1], M. Uğur TEOMAN[1], Niyazi TÜRKELLİ[1], Metin KAHRAMAN[1], Didem CAMBAZ[1], Ahu MUTLU[1], Sebastian ROST[2], Gregory A. HOUSEMAN[2], David A. THOMPSON[3], David CORNWELL[3], Murat UTKUCU[4] and Levent GÜLEN[4]

[1] B.U. Kandilli Observatory and Earthquake Research Institute,Department of Geophysics, Istanbul, Turkey

Corresponding author. Tel: + 90 216 516 33 56; fax: + 90 216 516 38 06.

E-mail adres: selda.altuncu@boun.edu.tr

[2]Leeds University, Institute of Geophysics and Tectonics, School of Earth and Environment, Leeds, United Kingdom

[3] School of Geoscience, University of Aberdeen, King's College, Aberdeen, United Kingdom

[4]Sakarya University, Geophysics Department, Sakarya

Abstract

With the aim of extensively investigating the crustal structure beneath the western segment of the North Anatolian Fault Zone where it splays into northern and southern branches, a

---

temporary seismic network (Dense array for North Anatolia-DANA) consisting of 70 stations was deployed in early May 2012 and operated for 18 months in the Sakarya region during the FaultLab experiment. Out of 2437 events contaminated by explosions, we extracted 1371 well located earthquakes. The enhanced station coverage having a nominal station spacing of 7 km, lead to a minimum magnitude calculation of 0.1. Horizontal and vertical location uncertainties within the array do not exceed 0.8 km and 0.9 km, respectively. We observe considerable seismic activity along both branches of the fault where the depth of the seismogenic zone was mostly confined to 15 km. Using our current earthquake catalogue we obtained a *b*-value of 1. We also mapped the *b*-value variation with depth and observed a gradual decrease. Furthermore, we determined the source parameters of 41 earthquakes with magnitudes greater than 1.8 using P-wave first motion polarity method. Regional Moment Tensor Inversion method was also applied to earthquakes with magnitudes greater than 3.0. Focal mechanism solutions confirm that Sakarya and its vicinity is stressed by a compressional regime showing a primarily oblique-slip motion character. Stress tensor analysis indicates that the maximum principal stress is aligned in WNW-ESE direction and the tensional axis is aligned in NNE-SSW direction.

1. Introduction

The North Anatolian Fault Zone (NAFZ) is a large-scale continental strike slip fault system extending from Karlıova Junction in the east towards the Aegean domain in the west cutting across the entire Northern Turkey **(Figure 1a)**. This major plate boundary accommodates most of the westward movement of the Anatolian Block. Recent GPS measurements revealed a maximum slip rate of approximately 24±1 mm/yr for the NAFZ and a counterclockwise rotation of the Anatolian Block (Reilinger *et al.*, 1997; 2000; McClusky *et al.*, 2000). The NAFZ displays a more or less linear character along most of its 1500 km length until it splays into two main strands east of the Almacık Mountains **(Figure 1b)**. The northern strand dissects the Adapazari basin and traverses the Marmara Sea reaching the Gulf of Saros (Şengör, 2005). The southern strand mostly remains on land and is not as well developed considering the shallower depth of associated basins (Duman et al, 2005). It extends through Pamukova and Iznik Lake and enters the Sea of Marmara at the Gulf of Gemlik. Both the northern and southern strands bound two regions of uplift: the Almacık Mountains and the Armutlu Peninsula.

The intense internal deformation has caused numerous destructive earthquakes along the NAFZ throughout the 20th century. The most recent İzmit (17 August 1999, Mw:7.4) and Düzce (12 November 1999, Mw:7.2) events are regarded as the western continuation of a major earthquake sequence which started with the 1939 Erzincan earthquake in eastern Turkey (Toksöz et al., 1979; Barka, 1996) rupturing a nearly 1000-km long segment of the NAFZ. The proximity and rapid succession of these major events strongly implies an interaction between sequence nucleation processes, yet the nature of this interaction is still widely debated. Historical seismicity indicates that the İzmit earthquake occurred in an area of Coulomb stress increase induced by major earthquakes and several authors have pointed out the static triggering role of the İzmit event on the Düzce Earthquake (Parsons et al., 2000; King et al., 2001; Utkucu et al., 2003). As shown in **Figure 1b**, the Izmit earthquake ruptured the northern branch of the NAFZ along four distinct structural segments, namely the Golcuk, Izmit-Sapanca, Sakarya and Karadere segments. Rupture lengths along each of these segment varied between 25 km and 36 km with observed dextral displacements of 1.5-5m (Barka et. al, 2000). These segments are separated by right releasing stepovers wider than 1 km and/or gaps in the fault trace (Langridge et al., 2002; Lettis et al., 2000). Further to the east, the Düzce earthquake formed an east-west striking 40 km long rupture with an average lateral displacement of 3.5 m, also including 9 km of rupture overlap with the eastern termination of the İzmit rupture (Akyüz et al., 2002; Hartleb et al., 2002; Duman et al., 2005). The Düzce rupture also consists of several segments separated by restraining stepovers. Both these earthquakes were recorded extremely well by seismology and satellite geodesy (INSAR and GPS), and the coseismic source models have been accurately determined (Wright et al., 2001; Burgmann et al., 2002).

In the present study, we primarily focus on the western segment of the NAFZ (**Figure 1a**) benefiting from a dataset collected from a dense seismic array (consisting of 70 temporary broadband seismic stations and an additional 8 stations from the permanent network) encompassing both the northern and southern strands of the fault covering part of the rupture area of 1999 İzmit and Düzce earthquakes. This array was mainly designed to determine the fine scale structure of the crust in this area and to image the structure of the NAFZ in the lower crust. With the help of this new and extensive data set, our main objective is to provide new insights on the most recent micro-seismic activity and the relevant *b*-value. Furthermore, we used our focal mechanism solutions in order to put additional constrains on the current stress orientation in this region.

2. Data and Methods

Within the framework of the FaultLab project which is funded by National Environment Research Council (NERC-UK), the DANA array consisting of 70 broadband stations (54 CMG6TD, 6 CMG3TD, 2 CMGESPD and 1 CMG40TD sensors provided by the SEIS-UK instrument pool) was deployed in the Sakarya-Adapazarı region and operated from early May 2012 to late September 2013. In order to further improve the station coverage, DANA includes seven additional CMG6TD broadband sensors surrounding the array and installed by KOERI/department of Geophysics with support from Boğaziçi University Research Fund. Eight permanent stations of KOERI (CMG3TDs) were also included in our analysis. Data were recorded at 50Hz sampling. The array was composed of six parallel lines forming a 2-D grid crossing both the northern and southern branches of NAFZ, supplemented by a further 7 stations arranged in an arc on the east side **(Figure 2a).** The nominal station spacing of the stations was 7 km, which was achieved for majority of the stations.

2.1. Micro-seismicity and b-value Analysis

Local events were visually identified and extracted from the continuous data. Event locations were determined using HYPO71 (Lee and Lahr, 1972) implemented in ZSAC, an interactive software package developed at KOERI (Yılmazer, 2012). A well constrained 1D velocity model (modified from Karabulut et al., 2011) was used in the location algorithm which is shown in Table 1. The station configuration of this experiment with dense station spacing significantly enhanced the event detection capability and allowed us to locate a total of 2437 seismic events with a minimum local magnitude (M_L) of 0.1 during the deployment of DANA network. M_L magnitudes for epicentral distances less than 200 km were calculated using the formula from Baumbach et al., (2003).

Due to the rapidly growing resource extraction industry, several active quarries and mining areas exist in the study area. In order to properly constrain the earthquake related seismicity, contaminations caused by any explosions and quarry blasts must be eliminated from the event catalogue. We performed a statistical time of day analysis by searching daytime events versus nighttime events and plotting them as a function of geographic location. Taking into account the origin times of the events presented by the histogram in Figure 3a, we selected the daytime interval between 08:00 and 16:00 separating the events into 8 hr day-night segments. The logarithmic ratio of daytime to nighttime events is defined by the Q_m parameter (Wiemer and Baer, 2000; Kekovali et al., 2011). The region was divided into different overlapping square cells and we found that a cell size of 5 km x 5km contained sufficient number of events to precisely identify the locations of quarry and mining areas. We limited our search to crustal events with depths less than 20 km and magnitudes smaller than 3.0. The result of our analysis shows that Q_m values vary from -0.57 to 4.17 **(Figure 3b)**. We determined the blast locations to have values of $Q_m \geq 2.5$. In order to test the accuracy of the analysis, we compared these locations with current satellite images. In general, a good correlation was observed suggesting that the daytime to nighttime ratio analysis can provide valuable information on the location of potential quarry and mining areas. This analysis eliminated mining related explosions from the catalog and we identified 1371 earthquakes **(Figure 2a**, list also given as supplementary material S1) following the discrimination process. The vast majority (~96%) of the earthquake depths are approximately confined to the upper 15 km of the crust as shown in the depth histogram given in Figure 2b. Moreover, a magnitude histogram in Figure 2c demonstrates the detection capability of DANA network. The majority of the horizontal and vertical location uncertainties were found to be less than 0.8 km and 0.9 km, respectively. However, towards the edges of the array where the station coverage is less dense, we observed relatively higher uncertainties (**Figure4a**). The vast majority of the average RMS arrival-time misfits were calculated within the range of 0.05-0.4 seconds as indicated in **Figure 4b**. Figure 4c demonstrates the $M_L$standard deviations which do not exceed 0.1 within the DANA array; however, towards the edges (42 events from cluster C in Figure 2a) we calculated magnitude errors within the range of 0.3-0.4. Overall, azimuthal gap values vary between 21º and 220º. Based on the travel time plots for 31595 Pg and 18416 Sg phase readings given in **Figure 5a,** we calculated average seismic velocities of 5.95 km/sec and 3.46 km/sec for Pg and Sg phases, respectively. We also extracted a Vp/Vs ratio of 1.713 from the Wadati diagram given in **Figure** 5b which is slightly lower than our starting value of 1.74.

We also performed a *b*-value analysis, a significant parameter to characterize seismicity in a tectonically active region. Physically, the *b*-value describes the proportion of seismic energy released by small versus large earthquakes; for a greater *b*-value the number of large magnitude earthquakes is fewer relative to the number of small earthquakes. It can be extracted from the slope of cumulative earthquake occurrence vs magnitude curve **(Figure 6).** Moreover, the state of stress has a major effect in determining the character of the magnitude–frequency distribution (Mori and Abercrombie, 1997; Toda et al., 1998). On average, *b* is close to unity for most seismically active regions (e.g. Froelich & Davis 1993) but can vary from 0.3-2.5 (El-Isa and Eaton, 2014). Low *b*-values are associated with major earthquakes (Öncel et al., 1996) and asperities subjected to high stress (Wiemer & Wyss 1997), whereas high values are related to decreased shear stress (Urbancic, 1992), extensional stress (Froelich and Davis, 1993), etc. In the present study, *b*-values are calculated using a maximum likelihood approach adopted in the ZMAP code (Utsu, 1999; Wiemer and Katsumata, 1999). Using the 1371 earthquakes in our data set, we calculated a magnitude completeness (Mc) value of 0.7 and a *b*-value of 1.0 ± 0.03 **(Figure 6b).** Mc calculation is based on the maximum curvature method (Wiemer and Wyss, 2000). Both values are remarkably lower than the comparable values for the KOERI catalogue spanning the same area and the operation period of the DANA array (Mc: 1.7; *b*-value 1.32 ± 0.06, **Figure 6a**).

2.2. Fault Plane Solutions and Stress Tensor Inversion

We applied the P-wave first arrival method from Suetsuge (1998) to obtain the fault plane parameters for earthquakes with moment magnitude $M_L \geq 1.8$ **(Table 2).** Furthermore, we also used the Regional Moment Tensor (RMT) inversion method of Dreger (2002) to infer the source parameters of the earthquakes with magnitudes greater than 3.0. This method adopts a least squares approach and makes use of full wave-form modeling which can provide reliable constraints on the source orientation using data from sparsely distributed broadband stations or even single broadband station (Dreger and Helmberger, 1993; Walter, 1993; Dreger and Woods, 2002). The earthquake fault plane parameters (strike, dip, and rake) and the seismic moment can be obtained directly from the moment tensor description. The preparation of data involved a quality check of the three component waveforms. Stations with recording gaps and signals with signal-to-noise ratio lower than 4.0 were eliminated. Synthetic seismograms were computed using a frequency wavenumber algorithm (Saika, 1994). Green's functions were computed using crustal structure from Karabulut et al, (2011). We obtained fault plane parameters of 41 earthquakes recorded within the operation period of the seismic network **(Table 2).** Solutions from both methods are in good agreement predominantly indicating right lateral strike-slip faulting along both branches of NAFZ with a few exceptions in the vicinity of Akyazı region where we observed normal faulting **(Figure 7).** A comparison of both methods for the Serdivan mainshock is given as a supplementary material (S4).

Fault plane solutions play a key role in determining the stress field orientation (Gephart and Forsyth, 1984; Michael, 1984; Gephart and Forsyth, 1990; Bohnhoff et al., 2004). We applied a stress analysis method developed by Gephart and Forsyth (1984) which was implemented in a focal mechanism stress inversion code (FMSI; Gephart and Forsyth, 1990). Generally speaking, stress is defined by three principal axes (σ_1, σ_2, σ_3) using a tensor description. The tectonic regime is directly related to the dip angles between these axes and the horizontal plane. The stress amplitude ratio~~rate~~ (R) defined by the equation $R=(\sigma_2-\sigma_1)/(\sigma_3-\sigma_1)$, is used to assess the dominant stress state and explain the overall relation between the principal axes. More detailed explanations on R are given by Bellier and Zoback (1995). The method is based on the relation between the σ_1, σ_2, σ_3 components and the pressure (P) tension (T) axes in accordance with the Anderson faulting theory (McKenzie 1970). FMSI calculates the parameters σ_1, σ_2, σ_3 and R for each event in the cluster assuming that spatial and temporal variations do not occur in the stationary stress field and slip occurs in the direction of the maximum resolved shear stress on the fault plane. In order to accurately constrain the stress field, we compiled the fault plane parameters obtained from the DANA network and various other studies (Öcal, 1960; Canıtez and Uçer, 1967; Nowroozi, 1972; Canıtez and Büyükaşıkoğlu, 1983; Taymaz et al., 1991; Örgülü, 2001; Kalafat, 2009).

Figure **8A** illustrates the stress tensor inversion results from the focal mechanism solutions of the 1999 İzmit earthquake and its aftershocks from previous studies (references in Table 2). As seen in **Figure 8A**, the inversions calculated the best fitting stress tensor with azimuth and plunge values of σ_1=(110, 0), σ_2=(201,58), σ_3=(20, 32), and stress amplitude ratio R=0.35 indicating a transtensional regime similar to the regime found by Kiratzi (2002) and Pınar et al., (2010). Inversions from the focal mechanisms obtained in this study resulted in a stress tensor with azimuth and plunge values of σ_1=(103, 27), σ_2=(256,61), σ_3=(7, 11), and stress amplitude ratio R=0.45 as given **in Figure 8B**. The measure of the reliability of the solution is the average misfit rotation angle calculated as 6.0^o. This value reflects how well the individual focal mechanisms fit the corresponding stress tensor. The greater the misfit angle, the less spatially homogeneous is the stress field (Pinar et al., 2010; Hardebeck and Hauksson, 2001).

3. Discussion and Conclusions

The installation of a dense array across the NAFZ significantly enhanced the event detection capability enabling us to accurately locate 1371earthquakes **(Figure 2a**) within the 18 months recording period which is a strong evidence of high seismic activity. Contaminations in the cataloque caused by blasts and mining activities were eliminated after careful inspection. The seismogenic zone in the region surrounding the NAFZ is approximately confined to the upper 15 km of the crust. During this seismic experiment we recorded a moderate size earthquake (M_L :4.1) close to the town of Serdivan on 7 July 2012 **(Figure 2a).** We recorded 29 aftershocks within the following two-month period with magnitudes varying from 0.4 to 2.2 (provided as supplementary material **S2 and S3**). The aftershock distribution and focal mechanism solutions suggest that this activity might indicate an unmapped continuation of a NE-SW oriented secondary fault located to the north of the İzmit-Sapanca segment of NAFZ **(Figures 2, 6)**. Based on our observations, a foreshock activity has started nearly a month before the Serdivan mainshock, including a magnitude 2.3 earthquake which occured approximately seven minutes prior to this earthquake (Provided as supplementary material **S3**).

The recorded seismicity pattern displays several distinctive features. Although the northern branch of NAFZ produces higher seismicity, we also located a considerable number of earthquakes along the southern branch, namely the Geyve Fault. In addition to the concentration of seismic activity along the north and south strands of the NAF, much seismicity is located further north and south of the major fault strands. We observe a strong, diffuse cluster of seismicity south of the Geyve fault (marked by a red ellipse B in Figure 2). The occurrence of a nearby moderate size earthquake following the DANA array pull-out (22.10.2014, ML:4.5, black star in **Figure 2a** is a further indication of the continuous seismic activity there. Further to the south of the Geyve fault, we observed a relatively diffuse cluster close to city of Bilecik (marked by a red ellipse C in Figure 2a) indicating fault zone related deformation away from the main fault. Two earthquake clusters were also mapped north of Sakarya, in good agreement with the most recent active fault map published by Emre et al., (2013) from General Directorate of Mineral Research and Exploration (MTA). We located another cluster in the vicinity of Akyazı at the junction of the Dokurcun fault, İzmit-Sakarya and Duzce-Karadere fault segments (ellipse A in Figure 2a) forming a structural discontinuity that contains several small scale faults, for which a higher rate of seismicity is expected. This cluster occurs in a region of Coulomb stress increase, as reported by Utkucu et al., 2003.

The active fault map by MTA (Emre et al., 2013) indicates many relatively small scale normal faults at the east of the Akyazı junction between the 1967 Mudurnu Valley and 1999 İzmit earthquake ruptures and the right stepping fault segments **(Figure 1b, and Figure 7).** Barka et al., (2002) also measured a ~5m surface displacement following the 1999 İzmit earthquake. Therefore relatively high *b*-values for the stepover area east of the junction should be expected due to structural heterogeneity (King 1986; Wiemer and Katsumata, 1999; Liu et al., 2003). The aftershock studies (Aktar, 2004; Özalaybey, 2002; Karabulut et al., 2002) indicate a cluster of earthquakes in the fault junction, emphasizing a stress accumulation following the İzmit earthquake. Calculation of the Coulomb stress change after the 1999 Düzce earthquake using all the large earthquakes also requires an increase in stresses for the Akyazı junction. Interestingly, field studies indicated an about 10 km-long surface rupture gap along the 1999 İzmit earthquake surface rupture in this region (Barka et al., 2002).. There had been virtually no seismicity at the junction area before the 1999 İzmit earthquake (Gülen et al,. 2002), switching to a high aftershock activity (Özalaybey et al., 2002., Pınar et al., 2010) following the earthquake. Our seismicity observations revealed that relatively high seismicity rates persist at the junction and may still be associated with aftershock activity of the 1999 Izmit rupture. Long lasting aftershock activity is not unusual and is supported by global observations (Stein and Liu, 2009; Parsons, 2009). It seems that both the redistribution of stresses following the mainshock and the static stresses imparted by the large earthquake rupture along the fault segments results in stress enhancement at the junction and the generation of long-lasting seismic activity.

As shown in Figure 6, we calculated a b-value of 1 for the DANA array. This result is in good agreement with the values revealed in a national report by Earthquake Engineering

Department of KOERI (Erdik et al., 2006). Figure 9 demonstrates the depth variation of the *b*-value extracted from our final earthquake catalogue (excluding the events with magnitude errors higher than 0.2). **Figure 9** also shows a gradual decrease in *b*-values with depth beneath the fault. Similar observations have also been reported for the San Andreas Fault in California (Mori and Abercrombie 1997; Wiemer and Wyss, 1997). The *b*-values tend to rise in the shallow crust possibly due to presence of weak sedimentary layers and lower confining pressure.

We determined the fault plane solutions of 41 earthquakes recorded within the array using RMT and P-wave first motion polarity methods **(Table 2).** Solutions reveal right lateral strike-slip faulting along both branches of NAFZ (**Figure 7)** with a few exceptions in the vicinity of Akyazı region where we observed normal faulting possibly due to the existence of stepovers **(Figure 1b).** RMT solutions for the 1999 Izmit and Düzce mainshocks show strike-slip faulting and NE-SW extension that is well correlated with the tectonic regime and the orientation of NAFZ **(Table 2).** Moreover, fault plane solutions of the M_L:4.1 Serdivan mainshock, its aftershocks and foreshocks demonstrate two distinct fault planes. The first one is NE-SW oriented dextral strike slip fault and the second one is NW-SE oriented sinistral strike slip fault. The active fault map of MTA (Emre et al., 2013) shows a NE-SW striking secondary fault in the vicinity of Serdivan seismic activity. Based on our findings, we therefore suggest that the main fault plane is aligned in NE-SW direction with dextral strike slip motion and the aftershock distribution marks the continuation of this fault.

Our stress tensor inversion results imply that maximum principal stress axes (σ_1) are roughly WNW-ESE oriented and the horizontal minimum compressive stress axis (σ_3) is NNE-SSW oriented (Figure 8B). The R-value calculated from the aftershock study of the 1999 İzmit earthquake (references in Table 2) varies within the 0-0.5 range and peaks at about 0.3 (Figure 8A). On the other hand, the R-value for the DANA survey peaks at a value closer to 0.5, emphasizing that strike-slip is the dominant type of faulting. These results indicate that the western part of the NAFZ is predominantly influenced by WNW compression and NNE extension of similar magnitudes.

The deployment of a dense array in the area of a complicated continental strike-slip fault allowed extremely low detection thresholds for micro-seismicity in the vicinity of recent major earthquakes. The detected seismicity allows further insight into the deformation of the Sakarya region and has highlighted several areas of previously unmapped active deformation.

Acknowledgements

Major funding was provided by the UK Natural Environment Research Council (NERC) under grant NE/I028017/1 and partially supported by Boğaziçi University Research Fund (BAP) under grant 6922. We would like to thank all the project members from the University of Leeds, Boğaziçi University, Kandilli Observatory, Aberdeen University and Sakarya University. I would also like to thank Prof. Ali Pinar and Dr. Kıvanç Kekovalı for their valuable comments. Some of the figures were generated by GMT software (Wessel and Smith ,1995).

References

Aktar, M., Ozalaybey, S., Ergin, M., Karabulut, H., Bouin, M.-P., Tapırdamaz C., Biçmen, F., Yörük, A., Bouchon, M., 2004. Spatial variation of aftershock activity across the rupture zone of the 17 August 1999 Izmit earthquake, Turkey. Tectonophysics, 391: 325-334.

Akyuz, H.S., Hartleb, R., Barka,A., Altunel, E., Sunal,G., Meyer,B., Armijo, R., 2002. Surface Rupture and Slip Distribution of the 12 November 1999 Duzce Earthquake (*M* 7.1), North Anatolian Fault, Bolu, Turkey. Bulletin of the Seismological Society of America, 92 (1): 61–66.

Barka, A., 1996. Slip distribution along the North Anatolian fault associated with large earthquakes of the period of the period 1939-1967. Bull. Seism. Soc. Am., 59:521–589.

Barka, A., S. Akyuz, E. Altunel, G. Sunal, Z. Cakir, A. Dikbas, B. Yerli,T. Rockwell, J. Dolan, and R. Hartleb 2000. The August 17, 1999 I˙zmit earthquake, *M* 7.4, Eastern Marmara region, Turkey: study of surface rupture and slip distribution, in The 1999 Izmit and Duzce Earthquakes: Preliminary Results. Istanbul Technical University:349 pp.

Barka, A., H. S. Akyuz, E. Altunel, G. Sunal, Z. Cakır, A. Dikbas¸, B. Yerli, R. Armijo, B. Meyer, J. B. de Chabalier, T. Rockwell, J. R. Dolan, R. Hartleb, T. Dawson, S. Christofferson, A. Tucker, T. Fumal, R. Langridge, H. Stenner,W. Lettis, J. Bachhuber, and W. Page, 2002. The surface rupture and slip distribution of the 17 August 1999 ˙Izmit earthquake (*M*7.4), North Anatolian Fault. Bull. Seismol. Soc. Am., 92: 43–60.

Bellier, O. and Zoback, M.,1995. Recent state of stress change in the Walker Lane zone western basin and Range Province-USA. Tectonics, 14: 564– 593.

Baumbach, M., Bindi, D., Grosser, H., Milkereit, C., Parolai, S., Wang, R., Karakısa, S., Zümbül, S., Zschau, J., 2003. Calibration of an ML Scale in Northwestern Turkey from 1999 Izmit Aftershocks. Bulletin of the Seismological Society of America, Vol. 93, No. 5, pp. 2289–2295.

Bohnhoff, M., Baisch, S., Harjes, H.-P., 2004. Fault mechanisms of induced seismicity at the superdeep German Continental Deep Drilling Program (KTB) borehole and their relation to fault structure and stress field. J. Geophys. Res. 109, B02309. doi:10.1029/2003JB002528.

Canıtez, N. and Üçer, S.B., 1967. Computer determinations for the fault plane solutions in And Near Anatolia. Tectonophysics, 4(3):235-244.

Bürgmann, R., Ayhan, M.A., Fielding, E.J., Wright, Y., McClusky,S., Aktug, B., Demir, C., Lenk, O., Urkezer, A., 2002. Deformation during the 12 November 1999, Düzce, Turkey Earthquake, from GPS and InSAR Data. Bull. Seismol. Soc. Am., 92:161-171.

Canıtez, N. and Büyükaşıkoğlu, S., 1984. Seismicity of the Sinop Nuclear Power Plant Site, Final Report, ITU, İstanbul.

Dreger, D.S. and Helmberger, D.V. , 1993. Determination of source at regional distances With single stations or sparse network data. J. Geophys. Res. 98: 8107-8125.

Dreger, D.S. (2002), Time-Domain Moment Tensor Inverse Code (TDMT_INVC) Release 1.1, (on internet www.seismo.berkeley.edu/~dreger).

Dreger, D. and Woods, B., 2002. Regional distance seismic moment tensors Of Nuclear explosions. Tectonophysics, 356:139-156.

Duman, T. Y., Emre, Ö., Doğan, A., Özalp, S., 2005. Step-Over and Bend Structures along the 1999 Duzce Earthquake Surface Rupture, North Anatolian Fault, Turkey. Bulletin of the Seismological Society of America, Vol. 95, No. 4:1250–1262, doi: 10.1785/0120040082.

El-Isa, Z.H., and Eaton, D.W, 2014. Spatiotemporal variations in the *b*-value of earthquakes magnitude-frequency distributions: Classifications and causes. Tectonophysics, Vol. 615-616: 1-11.

Emre, Ö., Duman, T. Y., Özalp, S., Elmacı, H., Olgun, Ş., Şaroğlu, F., 2013. Active fault map of Turkey with an explanatory text 1:1,25,000. General Directorate of Mineral Research and Exploration, Special Publication Series,30.

Erdik, M., Şeşetyan, K., Demircioğlu, M.B., Durukal, E., 2006. Ulaştırma Bakanlığı Demiryolları, Limanlar ve Havameydanları İnşaatı Genel Müdürlüğü Kıyı Yapıları, Demiryolları ve Havameydanları İnşaatları Deprem Teknik Yönetmeliği için Deprem Tehlikesi Belirlenmesi, Report, Boğaziçi University, Kandilli Observatory and Earthquake Research Institute, Department of Earthquake Engineering (In Turkish).

Froelich, H, C., and Davis, S., 1993. Teleseismic b values: or, much ado about 1.0. J. Geophys. Res., 98: 631-644.

Gephart, J.W., Forsyth, D. W., 1984. An Improved method for determining the regional stress tensor using earthquake focal mechanism data: Application to the San Fernando Earthquake Sequence. Journal of Geophysical Research, 89:9305-9320.

Gephart, J.W., Forsyth, D. W., 1990. FMSI: A FORTRAN Program for Inverting Fault/Slickenside and Earthquake focal mechanism data to obtain the regional stress tensor. Computer&Geoscience, 16: 953-989.

Gülen, L., Pınar, A., Kalafat, D., Özel, N., Horasan, G., Yılmazer, M., Işıkara, A.M., 2002.Surface fault breaks, aftershocks distribution, and rupture process of the 17 August 1999 Izmit, Turkey, earthquake. Bulletin of the Seismological Society of America 92:230–244.

Hardebeck, J. L., Hauksson, E., 2001. Stress Orientations Obtained from Earthquake Focal Mechanisms: What Are Appropriate Uncertainty Estimates?. Bulletin of the Seismological Society of America, 91(2): 250–262.

Hartleb, Ross D., Dolan, James F., Akyuz, H. Serdar, Dawson, Timothy E., Tucker, Allan Z., Yerli, B., Rockwell, Thomas K., Toraman, Erkan., Cakir, Z., Dikbaş, A., Altunel, E., 2002. Surface Rupture and Slip Distribution along the Karadere Segment of the 17 August 1999 Izmit and the Western Section of the 12 November 1999 Düzce, Turkey. Earthquakes Bulletin of the Seismological Society of America, 92 (1): 67–78.

Kalafat, D., Kekovalı, K., Guneş, Y., Yılmazer, M., Kara, M., Deniz, P., Berberoğlu, M., 2009. Turkiye ve çevresi Faylanma-Kaynak Parametreleri (MT) Kataloğu (1938- 2008)): A Cataloque of source parameters of moderate and strong earthquakes for Turkey and its surrounding area (1938-2008). Boğazici University Publications, No=1026, 43s., Bebek-İstanbul.

Karabulut, H., Bouin, M.-P., Bouchon, M.,Dietrich,M., Cornou, C., Aktar, M., 2002. The seismicty in the eastern Marmara Sea after the 17 August 1999 Izmit earthquake. Bull. seism. Soc. Am., 92: 387–393.

Karabulut, H., Schmittbuhl, J., Özalaybey, S., Lengliné, O., Kömeç Mutlu, A., Durand, V., Bouchon, M., Daniel, G., Bouin, M, P., 2011. Evolution of the seismicity in the eastern Marmara Sea a decade before and after the 17 August 1999 Izmit earthquake, Tectonophysics, 510,17-27.

Kekovali, K., Kalafat, D., Kara, M., Deniz, P., 2011. The estimation capability of potential mining and quarry areas from seismic catalog using statistical analysis, an application to Turkey. International Journal of the Physical Science Vol.6 (15):3704-3714.

King, G. C. P., 1986. Speculations on the geometry of the initiation and termination processes of earthquake rupture and its relation to morphology and geologic structure: Pure and Applied Geophysics, v. 124: 567-585.

King, G.C.P., Hubert-Ferrari, A., Nalbant, S.S., Meyer, B., Armijo, R., Bowman, D.,2001. Coulomb interactions and the 17 August 1999 _Izmit, Turkey earthquake. Earth Planet Sci 333:557–569.

Kiratzi, A. A., 2002. Stress tensor inversions along the westernmost North Anatolian Fault Zone and its continuation into the North Aegean Sea. Geophys. J. Int., 151: 360–376.

Langridge,R.M., H. D. Stenner, T. E. Fumal, S. A. Christofferson, T. K. Rockwell, R. D. Hartleb, J. Bachhuber, and A. A. Barka, 2002. Geometry, Slip Distribution, and Kinematics of Surface Rupture on the Sakarya Fault Segment during the 17 August 1999 Izmit, Turkey. Bulletin of the Seismological Society of America, 92 (1):107–125.

Lee WHK, Lahr JC (1972) HYPO71: a computer program for determining hypocenter, magnitude and first-motion pattern of local earthquakes. U.S. Geological survey open-file report: 100.

Lettis, W., J. Bachhuber, A. Barka, R. Witter, and C. Brankman., 2000. Surface fault rupture and segmentation during the Kocaeli Earthquake, in The 1999 Izmit and Duzce Earthquakes: Preliminary Results, A. Barka, O. Kozaci, S. Akyuz, and E. Altunel (Editors), Istanbul Technical University, Istanbul: 349.

Liu, J., Sieh, K., Hauksson, E., 2003. A Structural Interpretation of the Aftershock 'Cloud' of the 1992 Mw 7.3 Landers Earthquake. Bull. Seismol. Soc. America., (93)3:1333-1344.

Mckenzie, D.P., 1970. Plate tectonics of the Mediterranean region. Nature, 226,:239-243.

Mckenzie, D.P., 1972. Active Tectonics of the Mediterranean region. Geophys. J. R. Astr. Soc., 30: 109-185.

McClusky, S., Balassanian, S., Barka, A., Demir, C., Ergintav, S., Georgiev, I., Gurkan, O., Hamburger, M., Hurst, K., Kahle, H., Kastens, K., Kekelidze, G., King, R., Kotzev, V., Lenk, O., Mahmoud, S., Mishin, A., Nadariya, M., Ouzounis, A., Paradissis, D., Peter, Y., Prilepin, M., Reilinger, R., Sanli, I., Seeger, H., Tealeb, A., Toksöz, M.N., Veis, G., 2000. Global positioning system constraints on plate kinematics and dynamics in the eastern Mediterranean and Caucasus. J. Geophys. Res. 105: 5695–5719.

Michael, A.J., 1984. Determination of stress from slip data: faults and folds. J. Geophys. Res. 89 :517–526.

Mori, J., Abercrombie, R. E., 1997. Depth dependence of earthquake frequency-magnitude distrubutions in California: Implications for rupture initiation. Journal of Geophysical Research, 102 (15): 081-090.

Nowroozi, A.A. 1972. Focal Mechanism of Earthquakes in Persia, Turkey, west Pakistan and Afghanistan and plate tectonics of the midde east. Bull. Seismol. Soc. America., 62: 823-850.

Öcal, N., 1960. Determination of the Mechanism of some Anatolian Earthqaukes, A Symposium on eq. mechanism. Vol.24 (10): 365-370.

Öncel, A.O., Main, I.G., Alptekin, Ö ., Cowie, P., 1996. Temporal variations in the fractal properties of seismicity in the North Anatolian Fault Zone between 31^0N and 41^0E. Pure appl. Geophys., 146: 147–159.

Örgülü, G., Aktar, M., 2001. Regional moment tensor inversion for strong aftershocks of the August 17, 1999 Izmit earthquake (Mw=7.4). Geophys. Res. Lett. 28 (2): 371–374.

Özalaybey, S., Ergin, M., Aktar, M., Tapırdamaz, C., Biçmen, F., Yörük, A., 2002. The 1999 _Izmit earthquake sequence in Turkey: seismological and tectonic aspects. Bull Seismol Soc Am 92(1):376–386. doi: 10.1785/0120000838.

Parsons, T. (2009), Lasting earthquake legacy. Nature, v. 462: 41-42.

Parsons, T., Toda, S., Stein, R.S., Barka, A., Dieterich, J.H., 2000. Heightened odds of large earthquakes near Istanbul: an interaction-based probability calculation. Science 288:661–665. doi:10.1126/science.288.5466.661.

Pinar, A., Ucer, S.B., Honkura, Y., Sezgin, N., Ito, A., Baris, Ş., Kalafat, D., Matsushima,M. and S. Horiuchi, 2010. Spatial variation of stress field along the fault rupture zone of the 1999 Izmit Earthquake. Earth Planets Space, 61(3):237-256.

Reilinger, R. E., S. C. McClusky, and M. B. Oral, 1997. GPS measurements of present day crustal movements in the Arabia-Africa-Eurasia plate collision zone. J. Geophys. Res. , 102: 9983 –9999.

Reilinger, R. E., S. Ergintav, R. Burgmann, S. McClusky, O. Lenk, A. Barka, O. Gurkan, L. Hearn, K. L. Feigl, R. Cakmak, B. Aktug, H. Ozener, M. N. Toksoz, 2000. Coseismic and Postseismic Fault Slip for the 17 August 1999, M=7.5, Izmit, Turkey Earthquake. Science, 289: 1519–1524.

Saikia, C. K., 1994. Modified frequency-wavenumber algorithm for regional seismograms using Filon’s quadrature; modeling of Lg waves in eastern North America. Geophysical Journal International, 118: 142-158.

Suetsugu, D., 1998. Practise On Source Mechanism. IISEE Lecture Note. Tsukuba, Japan, p.104.

Stein, S., Liu, M., 2009. Long aftershock sequences within continents and implications for earthquake hazard assessment. Nature (Letters), vol:462:87-89.

Şengör, A.M.C., Tüysüz, O., İmren, C., Sakınç, M., Eyidoğan, H., Görür, N., Xavier Le Pichon, and Claude R., 2005. The North Anatolian Fault : A New Look Annual Review of Earth and Planetary Sciences, Vol. 33: 37-112 .

Taymaz, T., Jackson, J.A.,Mckenzie, D., 1991. Active Tectonics of the North and central Aegean Sea. Geophys. J. Int., 106: 433-490.

Toda, S., Stein, R.S., Reasenberg, P.A., Dieterich, J.H., 1998. Stress transferred by the Mw = 6.5 Kobe, Japan, shock: effect on aftershocks and future earthquake probabilities. Journal of Geophysical Research 103: 24543–24565.

Toksöz, M. N., Shakal A.F., Micheal A.J., 1979. Space-time migration of earthquakes along the North Anatolian Fault Zone and seismic gaps. Pure Appl Geophys 117:1258–1270. doi:10.1007/BF00876218.

Urbancic, T.I., Trifu, C.I., Long, J.M. & Toung, R.P., 1992. Space-time correlations of b-values with stress release. Pure appl. Geophys., 139: 449–462.

Utkucu, M., Nalbant, S., McClusky, J., Steacy, S., Alptekin, Ö., 2003. Slip distribution and stress changes associated with the 1999 November 12, Düzce (Turkey) earthquake (Mw = 7.1). Geophys J Int., 153:229–241. doi:10.1046/j.1365-246X.2003.01904.x

Utsu, T., 1999. Representation and analysis of the earthquake size distribution: a historical review and some new approaches. Pure Appl Geophys., 155:509–535.

Walter, R. W., 1993. Source parameters of the June 29, 1992 Little Skull Mountain earthquake from complete regional waveforms at single station. Geophys. Res. Lett., 20: 403-406.

Wessel, P., Smith, W.H.F., 1995. New version of the generic mapping tools (GMT). EOS Trans. 76: 329.

Wiemer S, Baer M., 2000. Mapping and removing quarry blast events from seismicity catalogs. Bull. Seismol. Soc. Am., 90(2): 525-530.

Wiemer S, Wyss M., 1997. Mapping the frequency-magnitude distribution in asperities: an improved technique to calculate recurrence times. Journal of Geophysical Research, 102:15115–15128. doi:10.1029/97JB00726.

Wiemer, S., Katsumata, K., 1999. Spatial variability of seismicity parameters in aftershock zones. Journal of Geophysical Research, 104: 13135–13151.

Wiemer, S., Wyss, M., 2000. Minumum magnitude of complete reporting in earthquake catalogs: examples from Alaska, the Western United States, and Japan, Bull. Seism. Soc. Am. 90, 859-869.

Wright, T., Parsons, B., Fielding, E., 2001. Measurement of interseismic strain accumulation across the North Anatolian Fault by satellite radar interferometry. Geophys. Res. Lett., 28:2117-2120.

Yılmazer M., 2012. zSacWin: A Rapid Earhquake Processing and Archiving System, User Guide v1.0. December 2012. Supported by the Research Fund of the Boğaziçi University Project Number 5725P.

Table Captions

Table 1: 1-D velocity model modified from Karabulut et al., (2011).

Table 2: The locations and source parameters of earthquakes (M≥1.8) in Sakarya region and surroundings compiled from our work and the previous studies. (1-McKenzie (1972), 2-Canıtez and Büyükaşıkoğlu (1984), 3-Canıtez and Uçer (1967), 4-Öcal (1960), 5- Nowroozi (1972), 6- Taymaz et al (1991), 7- Örgülü (2001), 8- Kalafat et al (2009), HRV- Harvard Centroid-Moment Tensor Project.

New constraints on micro-seismicity and stress state in the western part of the North Anatolian Fault Zone: Observations from a dense seismic array

Selda ALTUNCU POYRAZ [1], M. Uğur TEOMAN[1], Niyazi TÜRKELLİ[1], Metin KAHRAMAN[1], Didem CAMBAZ[1], Ahu MUTLU[1], Sebastian ROST[2], Gregory A. HOUSEMAN[2], David A. THOMPSON[3], David CORNWELL[3], Murat UTKUCU[4] and Levent GÜLEN[4]

[1] B.U. Kandilli Observatory and Earthquake Research Institute,Department of Geophysics, Istanbul, Turkey

Corresponding author. Tel: + 90 216 516 33 56; fax: + 90 216 516 38 06.

E-mail adres: selda.altuncu@boun.edu.tr

[2]Leeds University, Institute of Geophysics and Tectonics, School of Earth and Environment, Leeds, United Kingdom

[3] School of Geoscience, University of Aberdeen, King's College, Aberdeen, United Kingdom

[4]Sakarya University, Geophysics Department, Sakarya

Abstract

With the aim of extensively investigating the crustal structure beneath the western segment of the North Anatolian Fault Zone where it splays into northern and southern branches, a temporary seismic network (Dense array for North Anatolia-DANA) consisting of 70 stations was deployed in early May 2012 and operated for 18 months in the Sakarya region during the FaultLab experiment. Out of 2437 events contaminated by explosions, we extracted 1371 well located earthquakes. The enhanced station coverage having a nominal station spacing of 7 km, lead to a minimum magnitude calculation of 0.1. Horizontal and vertical location uncertainties within the array do not exceed 0.8 km and 0.9 km, respectively. We observe considerable seismic activity along both branches of the fault where the depth of the seismogenic zone was mostly confined to 15 km. Using our current earthquake catalogue we obtained a *b*-value of 1. We also mapped the *b*-value variation with depth and observed a gradual decrease. Furthermore, we determined the source parameters of 41 earthquakes with magnitudes greater than 1.8 using P-wave first motion polarity method. Regional Moment Tensor Inversion method was also applied to earthquakes with magnitudes greater than 3.0. Focal mechanism solutions confirm that Sakarya and its vicinity is stressed by a compressional regime showing a primarily oblique-slip motion character. Stress tensor analysis indicates that the maximum principal stress is aligned in WNW-ESE direction and the tensional axis is aligned in NNE-SSW direction.

1. Introduction

The North Anatolian Fault Zone (NAFZ) is a large-scale continental strike slip fault system extending from Karlıova Junction in the east towards the Aegean domain in the west cutting across the entire Northern Turkey **(Figure 1a)**. This major plate boundary accommodates most of the westward movement of the Anatolian Block. Recent GPS measurements revealed a maximum slip rate of approximately 24±1 mm/yr for the NAFZ and a counterclockwise rotation of the Anatolian Block (Reilinger *et al.*, 1997; 2000; McClusky *et al.*, 2000). The NAFZ displays a more or less linear character along most of its 1500 km length until it splays into two main strands east of the Almacık Mountains **(Figure 1b)**. The northern strand dissects the Adapazari basin and traverses the Marmara Sea reaching the Gulf of Saros (Şengör, 2005). The southern strand mostly remains on land and is not as well developed considering the shallower depth of associated basins (Duman et al, 2005). It extends through Pamukova and Iznik Lake and enters the Sea of Marmara at the Gulf of Gemlik. Both the northern and southern strands bound two regions of uplift: the Almacık Mountains and the Armutlu Peninsula.

The intense internal deformation has caused numerous destructive earthquakes along the NAFZ throughout the 20th century. The most recent İzmit (17 August 1999, Mw:7.4) and Düzce (12 November 1999, Mw:7.2) events are regarded as the western continuation of a major earthquake sequence which started with the 1939 Erzincan earthquake in eastern Turkey (Toksöz et al., 1979; Barka, 1996) rupturing a nearly 1000-km long segment of the NAFZ. The proximity and rapid succession of these major events strongly implies an interaction between sequence nucleation processes, yet the nature of this interaction is still widely debated. Historical seismicity indicates that the İzmit earthquake occurred in an area of Coulomb stress increase induced by major earthquakes and several authors have pointed out the static triggering role of the İzmit event on the Düzce Earthquake (Parsons et al., 2000; King et al., 2001; Utkucu et al., 2003). As shown in **Figure 1b**, the Izmit earthquake ruptured the northern branch of the NAFZ along four distinct structural segments, namely the Golcuk, Izmit-Sapanca, Sakarya and Karadere segments. Rupture lengths along each of these segment varied between 25 km and 36 km with observed dextral displacements of 1.5-5m (Barka et. al, 2000). These segments are separated by right releasing stepovers wider than 1 km and/or gaps in the fault trace (Langridge et al., 2002; Lettis et al., 2000). Further to the east, the Düzce earthquake formed an east-west striking 40 km long rupture with an average lateral displacement of 3.5 m, also including 9 km of rupture overlap with the eastern termination of the İzmit rupture (Akyüz et al., 2002; Hartleb et al., 2002; Duman et al., 2005). The Düzce rupture also consists of several segments separated by restraining stepovers. Both these earthquakes were recorded extremely well by seismology and satellite geodesy (INSAR and GPS), and the coseismic source models have been accurately determined (Wright et al., 2001; Burgmann et al., 2002).

In the present study, we primarily focus on the western segment of the NAFZ (**Figure 1a**) benefiting from a dataset collected from a dense seismic array (consisting of 70 temporary broadband seismic stations and an additional 8 stations from the permanent network) encompassing both the northern and southern strands of the fault covering part of the rupture area of 1999 İzmit and Düzce earthquakes. This array was mainly designed to determine the fine scale structure of the crust in this area and to image the structure of the NAFZ in the lower crust. With the help of this new and extensive data set, our main objective is to provide new insights on the most recent micro-seismic activity and the relevant *b*-value. Furthermore, we used our focal mechanism solutions in order to put additional constrains on the current stress orientation in this region.

2. Data and Methods

Within the framework of the FaultLab project which is funded by National Environment Research Council (NERC-UK), the DANA array consisting of 70 broadband stations (54 CMG6TD, 6 CMG3TD, 2 CMGESPD and 1 CMG40TD sensors provided by the SEIS-UK instrument pool) was deployed in the Sakarya-Adapazarı region and operated from early May 2012 to late September 2013. In order to further improve the station coverage, DANA includes seven additional CMG6TD broadband sensors surrounding the array and installed by KOERI/department of Geophysics with support from Boğaziçi University Research Fund. Eight permanent stations of KOERI (CMG3TDs) were also included in our analysis. Data were recorded at 50Hz sampling. The array was composed of six parallel lines forming a 2-D grid crossing both the northern and southern branches of NAFZ, supplemented by a further 7 stations arranged in an arc on the east side **(Figure 2a).** The nominal station spacing of the stations was 7 km, which was achieved for majority of the stations.

2.1. Micro-seismicity and b-value Analysis

Local events were visually identified and extracted from the continuous data. Event locations were determined using HYPO71 (Lee and Lahr, 1972) implemented in ZSAC, an interactive software package developed at KOERI (Yılmazer, 2012). A well constrained 1D velocity model (modified from Karabulut et al., 2011) was used in the location algorithm which is shown in Table 1. The station configuration of this experiment with dense station spacing significantly enhanced the event detection capability and allowed us to locate a total of 2437 seismic events with a minimum local magnitude (M_L) of 0.1 during the deployment of DANA network. M_L magnitudes for epicentral distances less than 200 km were calculated using the formula from Baumbach et al., (2003).

Due to the rapidly growing resource extraction industry, several active quarries and mining areas exist in the study area. In order to properly constrain the earthquake related seismicity, contaminations caused by any explosions and quarry blasts must be eliminated from the event catalogue. We performed a statistical time of day analysis by searching daytime events versus nighttime events and plotting them as a function of geographic location. Taking into account the origin times of the events presented by the histogram in Figure 3a, we selected the daytime interval between 08:00 and 16:00 separating the events into 8 hr day-night segments. The logarithmic ratio of daytime to nighttime events is defined by the Q_m parameter (Wiemer and Baer, 2000; Kekovali et al., 2011). The region was divided into different overlapping square cells and we found that a cell size of 5 km x 5km contained sufficient number of events to precisely identify the locations of quarry and mining areas. We limited our search to crustal events with depths less than 20 km and magnitudes smaller than 3.0. The result of our analysis shows that Q_m values vary from -0.57 to 4.17 **(Figure 3b)**. We determined the blast locations to have values of $Q_m \geq 2.5$. In order to test the accuracy of the analysis, we compared these locations with current satellite images. In general, a good correlation was observed suggesting that the daytime to nighttime ratio analysis can provide valuable information on the location of potential quarry and mining areas. This analysis eliminated mining related explosions from the catalog and we identified 1371 earthquakes **(Figure 2a**, list also given as supplementary material S1) following the discrimination process. The vast majority (~96%) of the earthquake depths are approximately confined to the upper 15 km of the crust as shown in the depth histogram given in Figure 2b. Moreover, a magnitude histogram in Figure 2c demonstrates the detection capability of DANA network. The majority of the horizontal and vertical location uncertainties were found to be less than 0.8 km and 0.9 km, respectively. However, towards the edges of the array where the station coverage is less dense, we observed relatively higher uncertainties (**Figure4a**). The vast majority of the average RMS arrival-time misfits were calculated within the range of 0.05-0.4 seconds as indicated in **Figure 4b**. Figure 4c demonstrates the $M_L$standard deviations which do not exceed 0.1 within the DANA array; however, towards the edges (42 events from cluster C in Figure 2a) we calculated magnitude errors within the range of 0.3-0.4. Overall, azimuthal gap values vary between 21º and 220º. Based on the travel time plots for 31595 Pg and 18416 Sg phase readings given in **Figure 5a,** we calculated average seismic velocities of 5.95 km/sec and 3.46 km/sec for Pg and Sg phases, respectively. We also extracted a Vp/Vs ratio of 1.713 from the Wadati diagram given in **Figure** 5b which is slightly lower than our starting value of 1.74.

We also performed a *b*-value analysis, a significant parameter to characterize seismicity in a tectonically active region. Physically, the *b*-value describes the proportion of seismic energy released by small versus large earthquakes; for a greater *b*-value the number of large magnitude earthquakes is fewer relative to the number of small earthquakes. It can be extracted from the slope of cumulative earthquake occurrence vs magnitude curve **(Figure 6).** Moreover, the state of stress has a major effect in determining the character of the magnitude–frequency distribution (Mori and Abercrombie, 1997; Toda et al., 1998). On average, *b* is close to unity for most seismically active regions (e.g. Froelich & Davis 1993) but can vary from 0.3-2.5 (El-Isa and Eaton, 2014). Low *b*-values are associated with major earthquakes (Öncel et al., 1996) and asperities subjected to high stress (Wiemer & Wyss 1997), whereas high values are related to decreased shear stress (Urbancic, 1992), extensional stress (Froelich and Davis, 1993), etc. In the present study, *b*-values are calculated using a maximum likelihood approach adopted in the ZMAP code (Utsu, 1999; Wiemer and Katsumata, 1999). Using the 1371 earthquakes in our data set, we calculated a magnitude completeness (Mc) value of 0.7 and a *b*-value of 1.0 ± 0.03 **(Figure 6b).** Mc calculation is based on the maximum curvature method (Wiemer and Wyss, 2000). Both values are remarkably lower than the comparable values for the KOERI catalogue spanning the same area and the operation period of the DANA array (Mc: 1.7; *b*-value 1.32 ± 0.06, **Figure 6a**).

2.2. Fault Plane Solutions and Stress Tensor Inversion

We applied the P-wave first arrival method from Suetsuge (1998) to obtain the fault plane parameters for earthquakes with moment magnitude $M_L \geq 1.8$ **(Table 2).** Furthermore, we also used the Regional Moment Tensor (RMT) inversion method of Dreger (2002) to infer the source parameters of the earthquakes with magnitudes greater than 3.0. This method adopts a least squares approach and makes use of full wave-form modeling which can provide reliable constraints on the source orientation using data from sparsely distributed broadband stations or even single broadband station (Dreger and Helmberger, 1993; Walter, 1993; Dreger and Woods, 2002). The earthquake fault plane parameters (strike, dip, and rake) and the seismic moment can be obtained directly from the moment tensor description. The preparation of data involved a quality check of the three component waveforms. Stations with recording gaps and signals with signal-to-noise ratio lower than 4.0 were eliminated. Synthetic seismograms were computed using a frequency wavenumber algorithm (Saika, 1994). Green's functions were computed using crustal structure from Karabulut et al, (2011). We obtained fault plane parameters of 41 earthquakes recorded within the operation period of the seismic network **(Table 2).** Solutions from both methods are in good agreement predominantly indicating right lateral strike-slip faulting along both branches of NAFZ with a few exceptions in the vicinity of Akyazı region where we observed normal faulting **(Figure 7).** A comparison of both methods for the Serdivan mainshock is given as a supplementary material (S4).

Fault plane solutions play a key role in determining the stress field orientation (Gephart and Forsyth, 1984; Michael, 1984; Gephart and Forsyth, 1990; Bohnhoff et al., 2004). We applied a stress analysis method developed by Gephart and Forsyth (1984) which was implemented in a focal mechanism stress inversion code (FMSI; Gephart and Forsyth, 1990). Generally speaking, stress is defined by three principal axes (σ_1, σ_2, σ_3) using a tensor description. The tectonic regime is directly related to the dip angles between these axes and the horizontal plane. The stress amplitude ratio (R) defined by the equation $R=(\sigma_2-\sigma_1)/(\sigma_3-\sigma_1)$, is used to assess the dominant stress state and explain the overall relation between the principal axes. More detailed explanations on R are given by Bellier and Zoback (1995). The method is based on the relation between the σ_1, σ_2, σ_3 components and the pressure (P) tension (T) axes in accordance with the Anderson faulting theory (McKenzie 1970). FMSI calculates the parameters σ_1, σ_2, σ_3 and R for each event in the cluster assuming that spatial and temporal variations do not occur in the stationary stress field and slip occurs in the direction of the maximum resolved shear stress on the fault plane. In order to accurately constrain the stress field, we compiled the fault plane parameters obtained from the DANA network and various other studies (Öcal, 1960; Canıtez and Uçer, 1967; Nowroozi, 1972; Canıtez and Büyükaşıkoğlu, 1983; Taymaz et al., 1991; Örgülü, 2001; Kalafat, 2009).

Figure **8A** illustrates the stress tensor inversion results from the focal mechanism solutions of the 1999 İzmit earthquake and its aftershocks from previous studies (references in Table 2). As seen in **Figure 8A**, the inversions calculated the best fitting stress tensor with azimuth and plunge values of σ_1=(110, 0), σ_2=(201,58), σ_3=(20, 32), and stress amplitude ratio R=0.35 indicating a transtensional regime similar to the regime found by Kiratzi (2002) and Pınar et al., (2010). Inversions from the focal mechanisms obtained in this study resulted in a stress tensor with azimuth and plunge values of σ_1=(103, 27), σ_2=(256,61), σ_3=(7, 11), and stress amplitude ratio R=0.45 as given **in Figure 8B**. The measure of the reliability of the solution is the average misfit rotation angle calculated as 6.0^o. This value reflects how well the individual focal mechanisms fit the corresponding stress tensor. The greater the misfit angle, the less spatially homogeneous is the stress field (Pinar et al., 2010; Hardebeck and Hauksson, 2001).

3. Discussion and Conclusions

The installation of a dense array across the NAFZ significantly enhanced the event detection capability enabling us to accurately locate 1371earthquakes **(Figure 2a**) within the 18 months recording period which is a strong evidence of high seismic activity. Contaminations in the cataloque caused by blasts and mining activities were eliminated after careful inspection. The seismogenic zone in the region surrounding the NAFZ is approximately confined to the upper 15 km of the crust. During this seismic experiment we recorded a moderate size earthquake (M_L :4.1) close to the town of Serdivan on 7 July 2012 **(Figure 2a).** We recorded 29 aftershocks within the following two-month period with magnitudes varying from 0.4 to 2.2 (provided as supplementary material **S2 and S3**). The aftershock distribution and focal mechanism solutions suggest that this activity might indicate an unmapped continuation of a NE-SW oriented secondary fault located to the north of the İzmit-Sapanca segment of NAFZ **(Figures 2, 6)**. Based on our observations, a foreshock activity has started nearly a month before the Serdivan mainshock, including a magnitude 2.3 earthquake which occured approximately seven minutes prior to this earthquake (Provided as supplementary material **S3**).

The recorded seismicity pattern displays several distinctive features. Although the northern branch of NAFZ produces higher seismicity, we also located a considerable number of earthquakes along the southern branch, namely the Geyve Fault. In addition to the concentration of seismic activity along the north and south strands of the NAF, much seismicity is located further north and south of the major fault strands. We observe a strong, diffuse cluster of seismicity south of the Geyve fault (marked by a red ellipse B in Figure 2). The occurrence of a nearby moderate size earthquake following the DANA array pull-out (22.10.2014, ML:4.5, black star in **Figure 2a** is a further indication of the continuous seismic activity there. Further to the south of the Geyve fault, we observed a relatively diffuse cluster close to city of Bilecik (marked by a red ellipse C in Figure 2a) indicating fault zone related deformation away from the main fault. Two earthquake clusters were also mapped north of Sakarya, in good agreement with the most recent active fault map published by Emre et al., (2013) from General Directorate of Mineral Research and Exploration (MTA). We located another cluster in the vicinity of Akyazı at the junction of the Dokurcun fault, İzmit-Sakarya and Duzce-Karadere fault segments (ellipse A in Figure 2a) forming a structural discontinuity that contains several small scale faults, for which a higher rate of seismicity is expected. This cluster occurs in a region of Coulomb stress increase, as reported by Utkucu et al., 2003.

The active fault map by MTA (Emre et al., 2013) indicates many relatively small scale normal faults at the east of the Akyazı junction between the 1967 Mudurnu Valley and 1999 İzmit earthquake ruptures and the right stepping fault segments **(Figure 1b, and Figure 7).** Barka et al., (2002) also measured a ~5m surface displacement following the 1999 İzmit earthquake. Therefore relatively high *b*-values for the stepover area east of the junction should be expected due to structural heterogeneity (King 1986; Wiemer and Katsumata, 1999; Liu et al., 2003). The aftershock studies (Aktar, 2004; Özalaybey, 2002; Karabulut et al., 2002) indicate a cluster of earthquakes in the fault junction, emphasizing a stress accumulation following the İzmit earthquake. Calculation of the Coulomb stress change after the 1999 Düzce earthquake using all the large earthquakes also requires an increase in stresses for the Akyazı junction. Interestingly, field studies indicated an about 10 km-long surface rupture gap along the 1999 İzmit earthquake surface rupture in this region (Barka et al., 2002).. There had been virtually no seismicity at the junction area before the 1999 İzmit earthquake (Gülen et al,. 2002), switching to a high aftershock activity (Özalaybey et al., 2002., Pınar et al., 2010) following the earthquake. Our seismicity observations revealed that relatively high seismicity rates persist at the junction and may still be associated with aftershock activity of the 1999 Izmit rupture. Long lasting aftershock activity is not unusual and is supported by global observations (Stein and Liu, 2009; Parsons, 2009). It seems that both the redistribution of stresses following the mainshock and the static stresses imparted by the large earthquake rupture along the fault segments results in stress enhancement at the junction and the generation of long-lasting seismic activity.

As shown in Figure 6, we calculated a b-value of 1 for the DANA array. This result is in good agreement with the values revealed in a national report by Earthquake Engineering

Department of KOERI (Erdik et al., 2006). Figure 9 demonstrates the depth variation of the *b*-value extracted from our final earthquake catalogue (excluding the events with magnitude errors higher than 0.2). **Figure 9** also shows a gradual decrease in *b*-values with depth beneath the fault. Similar observations have also been reported for the San Andreas Fault in California (Mori and Abercrombie 1997; Wiemer and Wyss, 1997). The *b*-values tend to rise in the shallow crust possibly due to presence of weak sedimentary layers and lower confining pressure.

We determined the fault plane solutions of 41 earthquakes recorded within the array using RMT and P-wave first motion polarity methods **(Table 2).** Solutions reveal right lateral strike-slip faulting along both branches of NAFZ (**Figure 7)** with a few exceptions in the vicinity of Akyazı region where we observed normal faulting possibly due to the existence of stepovers **(Figure 1b).** RMT solutions for the 1999 Izmit and Düzce mainshocks show strike-slip faulting and NE-SW extension that is well correlated with the tectonic regime and the orientation of NAFZ **(Table 2).** Moreover, fault plane solutions of the M_L:4.1 Serdivan mainshock, its aftershocks and foreshocks demonstrate two distinct fault planes. The first one is NE-SW oriented dextral strike slip fault and the second one is NW-SE oriented sinistral strike slip fault. The active fault map of MTA (Emre et al., 2013) shows a NE-SW striking secondary fault in the vicinity of Serdivan seismic activity. Based on our findings, we therefore suggest that the main fault plane is aligned in NE-SW direction with dextral strike slip motion and the aftershock distribution marks the continuation of this fault.

Our stress tensor inversion results imply that maximum principal stress axes (σ_1) are roughly WNW-ESE oriented and the horizontal minimum compressive stress axis (σ_3) is NNE-SSW oriented (Figure 8B). The R-value calculated from the aftershock study of the 1999 İzmit earthquake (references in Table 2) varies within the 0-0.5 range and peaks at about 0.3 (Figure 8A). On the other hand, the R-value for the DANA survey peaks at a value closer to 0.5, emphasizing that strike-slip is the dominant type of faulting. These results indicate that the western part of the NAFZ is predominantly influenced by WNW compression and NNE extension of similar magnitudes.

The deployment of a dense array in the area of a complicated continental strike-slip fault allowed extremely low detection thresholds for micro-seismicity in the vicinity of recent major earthquakes. The detected seismicity allows further insight into the deformation of the Sakarya region and has highlighted several areas of previously unmapped active deformation.

Acknowledgements

Major funding was provided by the UK Natural Environment Research Council (NERC) under grant NE/I028017/1 and partially supported by Boğaziçi University Research Fund (BAP) under grant 6922. We would like to thank all the project members from the University of Leeds, Boğaziçi University, Kandilli Observatory, Aberdeen University and Sakarya University. I would also like to thank Prof. Ali Pinar and Dr. Kıvanç Kekovalı for their valuable comments. Some of the figures were generated by GMT software (Wessel and Smith ,1995).

References

Aktar, M., Ozalaybey, S., Ergin, M., Karabulut, H., Bouin, M.-P., Tapırdamaz C., Biçmen, F., Yörük, A., Bouchon, M., 2004. Spatial variation of aftershock activity across the rupture zone of the 17 August 1999 Izmit earthquake, Turkey. Tectonophysics, 391: 325-334.

Akyuz, H.S., Hartleb, R., Barka,A., Altunel, E., Sunal,G., Meyer,B., Armijo, R., 2002. Surface Rupture and Slip Distribution of the 12 November 1999 Duzce Earthquake (*M* 7.1), North Anatolian Fault, Bolu, Turkey. Bulletin of the Seismological Society of America, 92 (1): 61–66.

Barka, A., 1996. Slip distribution along the North Anatolian fault associated with large earthquakes of the period of the period 1939-1967. Bull. Seism. Soc. Am., 59:521–589.

Barka, A., S. Akyuz, E. Altunel, G. Sunal, Z. Cakir, A. Dikbas, B. Yerli,T. Rockwell, J. Dolan, and R. Hartleb 2000. The August 17, 1999 I˙zmit earthquake, *M* 7.4, Eastern Marmara region, Turkey: study of surface rupture and slip distribution, in The 1999 Izmit and Duzce Earthquakes: Preliminary Results. Istanbul Technical University:349 pp.

Barka, A., H. S. Akyuz, E. Altunel, G. Sunal, Z. Cakır, A. Dikbas¸, B. Yerli, R. Armijo, B. Meyer, J. B. de Chabalier, T. Rockwell, J. R. Dolan, R. Hartleb, T. Dawson, S. Christofferson, A. Tucker, T. Fumal, R. Langridge, H. Stenner,W. Lettis, J. Bachhuber, and W. Page, 2002. The surface rupture and slip distribution of the 17 August 1999 ˙Izmit earthquake (*M*7.4), North Anatolian Fault. Bull. Seismol. Soc. Am., 92: 43–60.

Bellier, O. and Zoback, M.,1995. Recent state of stress change in the Walker Lane zone western basin and Range Province-USA. Tectonics, 14: 564– 593.

Baumbach, M., Bindi, D., Grosser, H., Milkereit, C., Parolai, S., Wang, R., Karakısa, S., Zümbül, S., Zschau, J., 2003. Calibration of an ML Scale in Northwestern Turkey from 1999 Izmit Aftershocks. Bulletin of the Seismological Society of America, Vol. 93, No. 5, pp. 2289–2295.

Bohnhoff, M., Baisch, S., Harjes, H.-P., 2004. Fault mechanisms of induced seismicity at the superdeep German Continental Deep Drilling Program (KTB) borehole and their relation to fault structure and stress field. J. Geophys. Res. 109, B02309. doi:10.1029/2003JB002528.

Canıtez, N. and Üçer, S.B., 1967. Computer determinations for the fault plane solutions in And Near Anatolia. Tectonophysics, 4(3):235-244.

Bürgmann, R., Ayhan, M.A., Fielding, E.J., Wright, Y., McClusky,S., Aktug, B., Demir, C., Lenk, O., Urkezer, A., 2002. Deformation during the 12 November 1999, Düzce, Turkey Earthquake, from GPS and InSAR Data. Bull. Seismol. Soc. Am., 92:161-171.

Canıtez, N. and Büyükaşıkoğlu, S., 1984. Seismicity of the Sinop Nuclear Power Plant Site, Final Report, ITU, İstanbul.

Dreger, D.S. and Helmberger, D.V. , 1993. Determination of source at regional distances With single stations or sparse network data. J. Geophys. Res. 98: 8107-8125.

Dreger, D.S. (2002), Time-Domain Moment Tensor Inverse Code (TDMT_INVC) Release 1.1, (on internet www.seismo.berkeley.edu/~dreger).

Dreger, D. and Woods, B., 2002. Regional distance seismic moment tensors Of Nuclear explosions. Tectonophysics, 356:139-156.

Duman, T. Y., Emre, Ö., Doğan, A., Özalp, S., 2005. Step-Over and Bend Structures along the 1999 Duzce Earthquake Surface Rupture, North Anatolian Fault, Turkey. Bulletin of the Seismological Society of America, Vol. 95, No. 4:1250–1262, doi: 10.1785/0120040082.

El-Isa, Z.H., and Eaton, D.W, 2014. Spatiotemporal variations in the *b*-value of earthquakes magnitude-frequency distributions: Classifications and causes. Tectonophysics, Vol. 615-616: 1-11.

Emre, Ö., Duman, T. Y., Özalp, S., Elmacı, H., Olgun, Ş., Şaroğlu, F., 2013. Active fault map of Turkey with an explanatory text 1:1,25,000. General Directorate of Mineral Research and Exploration, Special Publication Series,30.

Erdik, M., Şeşetyan, K., Demircioğlu, M.B., Durukal, E., 2006. Ulaştırma Bakanlığı Demiryolları, Limanlar ve Havameydanları İnşaatı Genel Müdürlüğü Kıyı Yapıları, Demiryolları ve Havameydanları İnşaatları Deprem Teknik Yönetmeliği için Deprem Tehlikesi Belirlenmesi, Report, Boğaziçi University, Kandilli Observatory and Earthquake Research Institute, Department of Earthquake Engineering (In Turkish).

Froelich, H, C., and Davis, S., 1993. Teleseismic b values: or, much ado about 1.0. J. Geophys. Res., 98: 631-644.

Gephart, J.W., Forsyth, D. W., 1984. An Improved method for determining the regional stress tensor using earthquake focal mechanism data: Application to the San Fernando Earthquake Sequence. Journal of Geophysical Research, 89:9305-9320.

Gephart, J.W., Forsyth, D. W., 1990. FMSI: A FORTRAN Program for Inverting Fault/Slickenside and Earthquake focal mechanism data to obtain the regional stress tensor. Computer&Geoscience, 16: 953-989.

Gülen, L., Pınar, A., Kalafat, D., Özel, N., Horasan, G., Yılmazer, M., Işıkara, A.M., 2002.Surface fault breaks, aftershocks distribution, and rupture process of the 17 August 1999 Izmit, Turkey, earthquake. Bulletin of the Seismological Society of America 92:230–244.

Hardebeck, J. L., Hauksson, E., 2001. Stress Orientations Obtained from Earthquake Focal Mechanisms: What Are Appropriate Uncertainty Estimates?. Bulletin of the Seismological Society of America, 91(2): 250–262.

Hartleb, Ross D., Dolan, James F., Akyuz, H. Serdar, Dawson, Timothy E., Tucker, Allan Z., Yerli, B., Rockwell, Thomas K., Toraman, Erkan., Cakir, Z., Dikbaş, A., Altunel, E., 2002. Surface Rupture and Slip Distribution along the Karadere Segment of the 17 August 1999 Izmit and the Western Section of the 12 November 1999 Düzce, Turkey. Earthquakes Bulletin of the Seismological Society of America, 92 (1): 67–78.

Kalafat, D., Kekovalı, K., Guneş, Y., Yılmazer, M., Kara, M., Deniz, P., Berberoğlu, M., 2009. Turkiye ve çevresi Faylanma-Kaynak Parametreleri (MT) Kataloğu (1938- 2008)): A Cataloque of source parameters of moderate and strong earthquakes for Turkey and its surrounding area (1938-2008). Boğazici University Publications, No=1026, 43s., Bebek-İstanbul.

Karabulut, H., Bouin, M.-P., Bouchon, M.,Dietrich,M., Cornou, C., Aktar, M., 2002. The seismicty in the eastern Marmara Sea after the 17 August 1999 Izmit earthquake. Bull. seism. Soc. Am., 92: 387–393.

Karabulut, H., Schmittbuhl, J., Özalaybey, S., Lengliné, O., Kömeç Mutlu, A., Durand, V., Bouchon, M., Daniel, G., Bouin, M, P., 2011. Evolution of the seismicity in the eastern Marmara Sea a decade before and after the 17 August 1999 Izmit earthquake, Tectonophysics, 510,17-27.

Kekovali, K., Kalafat, D., Kara, M., Deniz, P., 2011. The estimation capability of potential mining and quarry areas from seismic catalog using statistical analysis, an application to Turkey. International Journal of the Physical Science Vol.6 (15):3704-3714.

King, G. C. P., 1986. Speculations on the geometry of the initiation and termination processes of earthquake rupture and its relation to morphology and geologic structure: Pure and Applied Geophysics, v. 124: 567-585.

King, G.C.P., Hubert-Ferrari, A., Nalbant, S.S., Meyer, B., Armijo, R., Bowman, D.,2001. Coulomb interactions and the 17 August 1999 _Izmit, Turkey earthquake. Earth Planet Sci 333:557–569.

Kiratzi, A. A., 2002. Stress tensor inversions along the westernmost North Anatolian Fault Zone and its continuation into the North Aegean Sea. Geophys. J. Int., 151: 360–376.

Langridge,R.M., H. D. Stenner, T. E. Fumal, S. A. Christofferson, T. K. Rockwell, R. D. Hartleb, J. Bachhuber, and A. A. Barka, 2002. Geometry, Slip Distribution, and Kinematics of Surface Rupture on the Sakarya Fault Segment during the 17 August 1999 Izmit, Turkey. Bulletin of the Seismological Society of America, 92 (1):107–125.

Lee WHK, Lahr JC (1972) HYPO71: a computer program for determining hypocenter, magnitude and first-motion pattern of local earthquakes. U.S. Geological survey open-file report: 100.

Lettis, W., J. Bachhuber, A. Barka, R. Witter, and C. Brankman., 2000. Surface fault rupture and segmentation during the Kocaeli Earthquake, in The 1999 Izmit and Duzce Earthquakes: Preliminary Results, A. Barka, O. Kozaci, S. Akyuz, and E. Altunel (Editors), Istanbul Technical University, Istanbul: 349.

Liu, J., Sieh, K., Hauksson, E., 2003. A Structural Interpretation of the Aftershock ‘Cloud’ of the 1992 Mw 7.3 Landers Earthquake. Bull. Seismol. Soc. America., (93)3:1333-1344.

Mckenzie, D.P., 1970. Plate tectonics of the Mediterranean region. Nature, 226,:239-243.

Mckenzie, D.P., 1972. Active Tectonics of the Mediterranean region. Geophys. J. R. Astr. Soc., 30: 109-185.

McClusky, S., Balassanian, S., Barka, A., Demir, C., Ergintav, S., Georgiev, I., Gurkan, O., Hamburger, M., Hurst, K., Kahle, H., Kastens, K., Kekelidze, G., King, R., Kotzev, V., Lenk, O., Mahmoud, S., Mishin, A., Nadariya, M., Ouzounis, A., Paradissis, D., Peter, Y., Prilepin, M., Reilinger, R., Sanli, I., Seeger, H., Tealeb, A., Toksöz, M.N., Veis, G., 2000. Global positioning system constraints on plate kinematics and dynamics in the eastern Mediterranean and Caucasus. J. Geophys. Res. 105: 5695–5719.

Michael, A.J., 1984. Determination of stress from slip data: faults and folds. J. Geophys. Res. 89 :517–526.

Mori, J., Abercrombie, R. E., 1997. Depth dependence of earthquake frequency-magnitude distrubutions in California: Implications for rupture initiation. Journal of Geophysical Research, 102 (15): 081-090.

Nowroozi, A.A. 1972. Focal Mechanism of Earthquakes in Persia, Turkey, west Pakistan and Afghanistan and plate tectonics of the midde east. Bull. Seismol. Soc. America., 62: 823-850.

Öcal, N., 1960. Determination of the Mechanism of some Anatolian Earthqaukes, A Symposium on eq. mechanism. Vol.24 (10): 365-370.

Öncel, A.O., Main, I.G., Alptekin, Ö ., Cowie, P., 1996. Temporal variations in the fractal properties of seismicity in the North Anatolian Fault Zone between 31^0N and 41^0E. Pure appl. Geophys., 146: 147–159.

Örgülü, G., Aktar, M., 2001. Regional moment tensor inversion for strong aftershocks of the August 17, 1999 Izmit earthquake (Mw=7.4). Geophys. Res. Lett. 28 (2): 371–374.

Özalaybey, S., Ergin, M., Aktar, M., Tapırdamaz, C., Biçmen, F., Yörük, A., 2002. The 1999 _Izmit earthquake sequence in Turkey: seismological and tectonic aspects. Bull Seismol Soc Am 92(1):376–386. doi: 10.1785/0120000838.

Parsons, T. (2009), Lasting earthquake legacy. Nature, v. 462: 41-42.

Parsons, T., Toda, S., Stein, R.S., Barka, A., Dieterich, J.H., 2000. Heightened odds of large earthquakes near Istanbul: an interaction-based probability calculation. Science 288:661–665. doi:10.1126/science.288.5466.661.

Pinar, A., Ucer, S.B., Honkura, Y., Sezgin, N., Ito, A., Baris, Ş., Kalafat, D., Matsushima,M. and S. Horiuchi, 2010. Spatial variation of stress field along the fault rupture zone of the 1999 Izmit Earthquake. Earth Planets Space, 61(3):237-256.

Reilinger, R. E., S. C. McClusky, and M. B. Oral, 1997. GPS measurements of present day crustal movements in the Arabia-Africa-Eurasia plate collision zone. J. Geophys. Res. , 102: 9983 –9999.

Reilinger, R. E., S. Ergintav, R. Burgmann, S. McClusky, O. Lenk, A. Barka, O. Gurkan, L. Hearn, K. L. Feigl, R. Cakmak, B. Aktug, H. Ozener, M. N. Toksoz, 2000. Coseismic and Postseismic Fault Slip for the 17 August 1999, M=7.5, Izmit, Turkey Earthquake. Science, 289: 1519–1524.

Saikia, C. K., 1994. Modified frequency-wavenumber algorithm for regional seismograms using Filon's quadrature; modeling of Lg waves in eastern North America. Geophysical Journal International, 118: 142-158.

Suetsugu, D., 1998. Practise On Source Mechanism. IISEE Lecture Note. Tsukuba, Japan, p.104.

Stein, S., Liu, M., 2009. Long aftershock sequences within continents and implications for earthquake hazard assessment. Nature (Letters), vol:462:87-89.

Şengör, A.M.C., Tüysüz, O., İmren, C., Sakınç, M., Eyidoğan, H., Görür, N., Xavier Le Pichon, and Claude R., 2005. The North Anatolian Fault : A New Look Annual Review of Earth and Planetary Sciences, Vol. 33: 37-112 .

Taymaz, T., Jackson, J.A.,Mckenzie, D., 1991. Active Tectonics of the North and central Aegean Sea. Geophys. J. Int., 106: 433-490.

Toda, S., Stein, R.S., Reasenberg, P.A., Dieterich, J.H., 1998. Stress transferred by the Mw = 6.5 Kobe, Japan, shock: effect on aftershocks and future earthquake probabilities. Journal of Geophysical Research 103: 24543–24565.

Toksöz, M. N., Shakal A.F., Micheal A.J., 1979. Space-time migration of earthquakes along the North Anatolian Fault Zone and seismic gaps. Pure Appl Geophys 117:1258–1270. doi:10.1007/BF00876218.

Urbancic, T.I., Trifu, C.I., Long, J.M. & Toung, R.P., 1992. Space-time correlations of b-values with stress release. Pure appl. Geophys., 139: 449–462.

Utkucu, M., Nalbant, S., McClusky, J., Steacy, S., Alptekin, Ö., 2003. Slip distribution and stress changes associated with the 1999 November 12, Düzce (Turkey) earthquake (Mw = 7.1). Geophys J Int., 153:229–241. doi:10.1046/j.1365-246X.2003.01904.x

Utsu, T., 1999. Representation and analysis of the earthquake size distribution: a historical review and some new approaches. Pure Appl Geophys., 155:509–535.

Walter, R. W., 1993. Source parameters of the June 29, 1992 Little Skull Mountain earthquake from complete regional waveforms at single station. Geophys. Res. Lett., 20: 403-406.

Wessel, P., Smith, W.H.F., 1995. New version of the generic mapping tools (GMT). EOS Trans. 76: 329.

Wiemer S, Baer M., 2000. Mapping and removing quarry blast events from seismicity catalogs. Bull. Seismol. Soc. Am., 90(2): 525-530.

Wiemer S, Wyss M., 1997. Mapping the frequency-magnitude distribution in asperities: an improved technique to calculate recurrence times. Journal of Geophysical Research, 102:15115–15128. doi:10.1029/97JB00726.

Wiemer, S., Katsumata, K., 1999. Spatial variability of seismicity parameters in aftershock zones. Journal of Geophysical Research, 104: 13135–13151.

Wiemer, S., Wyss, M., 2000. Minumum magnitude of complete reporting in earthquake catalogs: examples from Alaska, the Western United States, and Japan, Bull. Seism. Soc. Am. 90, 859-869.

Wright, T., Parsons, B., Fielding, E., 2001. Measurement of interseismic strain accumulation across the North Anatolian Fault by satellite radar interferometry. Geophys. Res. Lett., 28:2117-2120.

Yılmazer M., 2012. zSacWin: A Rapid Earhquake Processing and Archiving System, User Guide v1.0. December 2012. Supported by the Research Fund of the Boğaziçi University Project Number 5725P.

Table Captions

Table 1: 1-D velocity model modified from Karabulut et al., (2011).

Table 2: The locations and source parameters of earthquakes (M≥1.8) in Sakarya region and surroundings compiled from our work and the previous studies. (1-McKenzie (1972), 2-Canıtez and Büyükaşıkoğlu (1984), 3-Canıtez and Uçer (1967), 4-Öcal (1960), 5- Nowroozi (1972), 6- Taymaz et al (1991), 7- Örgülü (2001), 8- Kalafat et al (2009), HRV- Harvard Centroid-Moment Tensor Project.

Table1

Depth (km)	V_p (km/s)
0	3.27
2	5.75
4	5.85
6	5.90
8	5.91
12	6.15
16	6.50
20	6.84
24	6.84
28	6.84
30	6.84
32	7.34
36	7.89
40	7.89

Table2

Click here to download Table: Table2.docx

no	*Date (d.m.y)*	*Time-GMT (h.m.s)*	*Latitute (N)*	*Longitute (E)*	M_L	M_w	*h(km)*	*Plane 1*			*Reference*
								Strike	*Dip*	*Rake*	
1	20.06.1943	15:32:54	40.85	30.51	6.2	6.4	10	176	76	2	1,2
2	20.02.1956	20:31:43	39.89	30.49	6.0	6.2	40	264	50	-133	1,3
3	26.05.1957	06:33:35	40.67	31.00	6.6	6.7	10	87	78	176	1,2,3,4
4	22.07.1967	16:56:58	40.67	30.69	6.3	6.2	33	93	90	176	1,5,6
5	22.07.1967	17:48:06	40.66	30.62	4.9	5.2	26	110	72	-17	8
6	17.08.1999	03:14:01	40.60	30.63	5.5	5.3	8	192	34	-82	7
7	17.08.1999	05:10:08	40.72	30.01	4.6	4.7	6	29	80	-173	7
8	17.08.1999	05:45:23	40.74	30.01	4.7	4.3	11	243	45	-163	7
9	17.08.1999	06:01:32	40.75	29.99	4.0	4.1	4	263	69	147	7
10	17.08.1999	00:01:37	40.75	29.86	--	7.6	17	91	87	164	HRV,USGS
11	18.08.1999	01:04:25	40.66	30.77	4.0	4.0	6	182	39	-77	7
12	19.08.1999	13:04:13	40.64	30.58	4.0	4.5	9	195	53	-83	7
13	20.08.1999	15:59:02	40.78	30.93	4.1	4.1	10	246	57	150	7
14	22.08.1999	14:31:00	40.67	30.77	4.4	4.1	9	276	72	-165	7
15	31.08.1999	18:10:51	40.75	29.97	4.6	5.0	11	82	71	-133	7
16	31.08.1999	08:33:25	40.74	29.97	4.2	4.4	11	68	70	-142	7
17	04.09.1999	10:30:53	40.73	30.02	4.0	4.0	13	224	43	153	7
18	13.09.1999	11:55:28	40.31	30.29	--	5.8	15	176	86	-31	HRV
19	17.09.1999	19:50:07	40.75	30.08	4.5	4.4	18	170	82	-21	7
20	07.11.1999	16:54:42	40.57	31.36	--	5.0	15	269	71	106	HRV
21	11.11.1999	14:41:25	40.95	30.10	--	5.7	15	208	86	-41	HRV
22	12.11.1999	16:57:20	40.76	31.16	--	7.2	10	170	80	-36	HRV,USGS
23	23.08.2000	13:41:27	40.68	30.72	--	5.3	15	152	74	-34	HRV
24	17.09.2002	12:05:00	40.81	30.58	--	3.7	6	237	59	-95	8
25	01.04.2003	07:51:00	40.73	30.68	--	3.9	8	21	78	-19	8
26	22.06.2011	14:00:52	40.5623	31.1257	3.0		5.0	325	87	-72	FaultLab
27	11.07.2011	16:09:11	40.1562	29.9545	4.6		6.0	105	77	-66	FaultLab
28	24.02.2012	06:56:05	40.6382	30.5040	2.8		1.8	259	76	-168	FaultLab
29	11.06.2012	15:00:05	40.8982	30.4223	1.9		4.6	17	81	-178	FaultLab
30	12.06.2012	12:22:50	40.7682	30.4058	2.2		5.0	215	69	-175	FaultLab
31	22.06.2012	01:57:55	39.8902	30.6258	2.7		5.0	47	45	-43	FaultLab
32	28.06.2012	17:46:07	40.4862	30.1423	2.1		6.8	77	88	163	FaultLab
33	01.07.2012	06:06:30	40.7750	30.8367	2.2		7.5	56	58	158	FaultLab
34	07.07.2012	07:07:45	40.7643	30.3798	4.1	4.1	6.0	218	74	-178	FaultLab
35	07.07.2012	06:56:02	40.7632	30.3962	2.0		11.6	16	89	164	FaultLab
36	07.07.2012	07:14:25	40.7642	30.3925	2.2		11.6	203	86	172	FaultLab
37	07.07.2012	07:24:34	40.7635	30.3978	1.9		10.8	223	72	175	FaultLab
38	07.07.2012	09:20:12	40.7632	30.3918	1.9		9.8	208	83	-176	FaultLab
39	10.07.2012	09:13:42	40.4580	30.0448	2.6		9.4	236	83	-175	FaultLab

40	16.07.2012	07:41:59	40.7465	30.7723	2.2		9.0	59	89	158	FaultLab
41	17.08.2012	08:03:23	40.7623	30.3988	1.9		8.8	66	82	134	FaultLab
42	14.10.2012	08:36:39	40.7048	30.3037	2.6		11.6	143	54	154	FaultLab
43	24.10.2012	01:03:59	40.7027	30.6742	2.1		8.1	22	56	-162	FaultLab
44	02.11.2012	13:19:09	40.7672	30.3870	2.2		9.2	47	83	-163	FaultLab
45	09.11.2012	20:03:53	40.6978	30.6255	2.1		11.9	338	79	-69	FaultLab
46	13.11.2012	18:17:30	40.7173	30.1558	2.1		4.9	3	49	-8	FaultLab
47	16.11.2012	01:54:57	39.8087	30.5162	3.5		5.0	125	68	-66	FaultLab
48	09.12.2012	04:45:36	40.6930	30.6233	3.5	3.5	5.0	335	73	-64	FaultLab
49	09.12.2012	13:58:37	40.7105	30.6667	2.0		10.8	72	68	-143	FaultLab
50	18.01.2013	03:04:20	40.6977	30.6270	2.0		10.3	359	67	-5	FaultLab
51	23.01.2013	12:44:48	40.3977	30.1605	2.6		1.8	53	89	-172	FaultLab
52	14.02.2013	17:54:37	40.8797	30.6942	2.7		12	82	79	-147	FaultLab
53	24.02.2013	05:09:06	40.7563	30.2688	2.5		11.4	257	88	-174	FaultLab
54	26.02.2013	04:04:54	40.7533	30.2730	2.0		11.3	259	86	-172	FaultLab
55	07.03.2013	09:22:15	40.5693	30.5390	2.5		5.2	11	68	-151	FaultLab
56	13.04.2013	07:33:48	40.5198	30.4830	1.9		6.9	354	79	11	FaultLab
57	23.04.2013	15:19:56	40.7597	30.3650	3.2	3.1	2.0	41	74	-150	FaultLab
58	09.05.2013	03:52:56	40.5760	30.5427	2.3		3.1	30	84	-131	FaultLab
59	22.05.2013	22:38:47	40.6917	30.6463	2.0		9.8	105	53	-120	FaultLab
60	27.05.2013	06:38:30	40.6862	30.4180	1.9		6.9	341	59	-144	FaultLab
61	02.06.2013	22:58:03	40.7137	30.1447	2.0		5.0	11	72	-33	FaultLab
62	08.06.2013	12:08:55	40.6862	30.5387	2.3		11.9	36	71	-133	FaultLab
63	30.06.2013	02:53:56	40.6850	30.6542	1.8		14.6	254	88	133	FaultLab
64	30.06.2013	03:22:06	40.6882	30.6097	3.2		3.5	9	77	-59	FaultLab
65	02.07.2013	01:45:09	40.7897	30.7195	2.1		8.0	19	65	13	FaultLab
66	10.11.2013	02:09:24	40.7417	30.2575	3.5	3.4	9.6	265	87	-49	FaultLab

Figure Captions

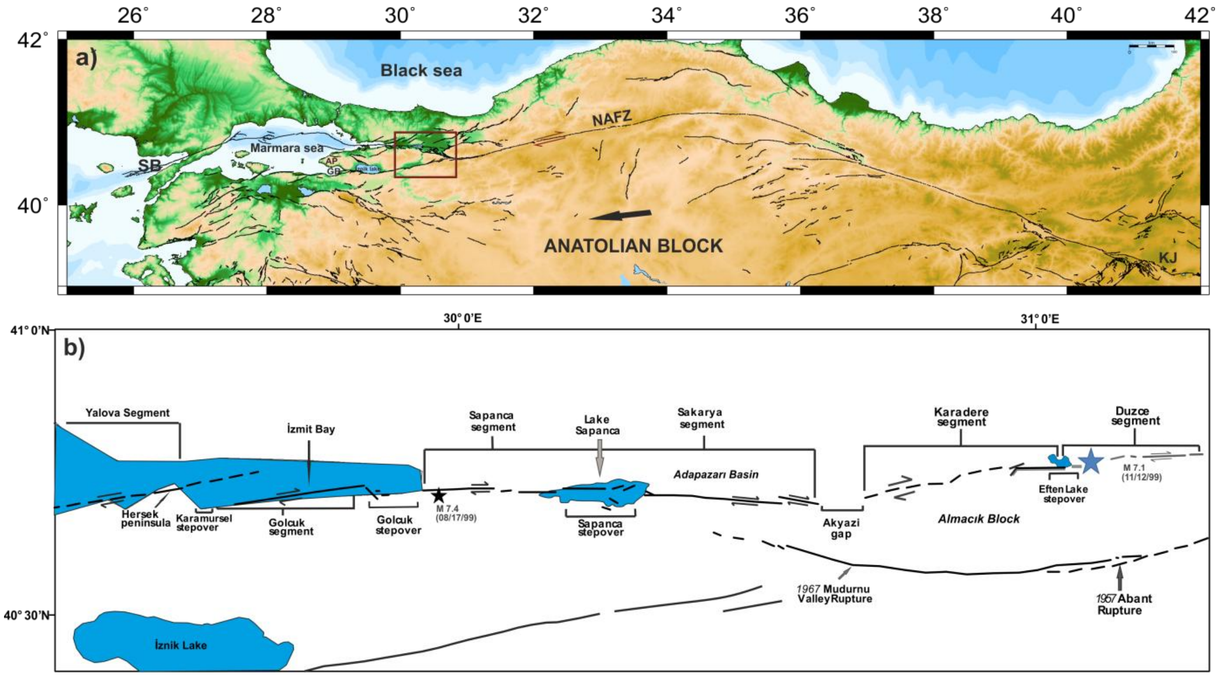

Figure 1: a) Topographic map of the North Anatolian Fault Zone (NAFZ) region. Study area is marked by a red square. Abbreviations; AP: Armutlu Peninsula, GB: Gemlik Bay, KJ: Karlıova Junction, SB:Saros Bay **b)** Locations of fault ruptures associated with major earthquakes in the western segment of NAFZ (modified from Lettis et al., 2002).

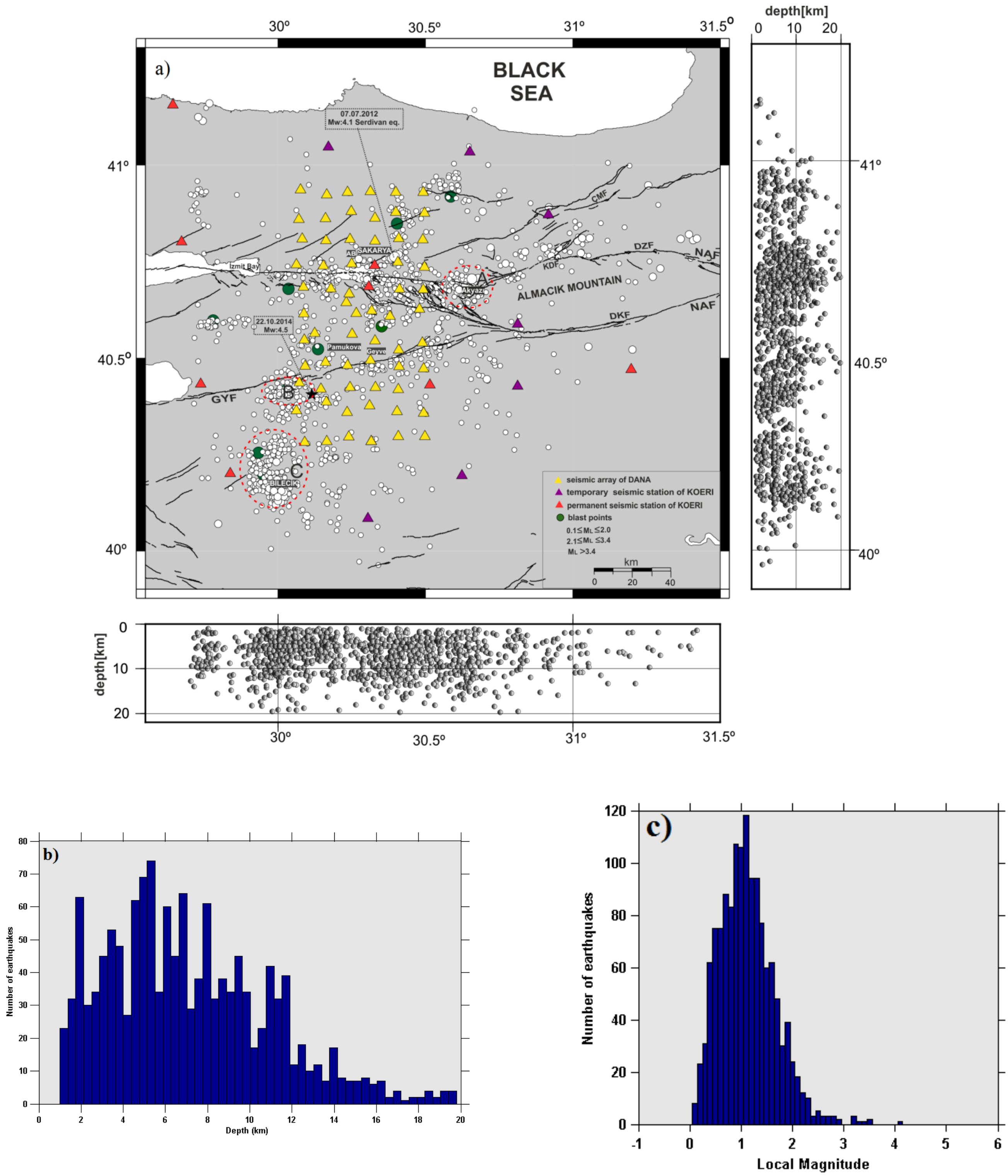

Figure 2: a) Local seismicity from May 2012 to September 2013. Most recent fault information is taken from Emre et al., 2013**.** Abbreviations; ÇMF: Çilimli Fault, DB: Düzce Basin, DKF:Dokurcun Fault, DZF:Düzce Fault, GYF:Geyve Fault, KDF: Karadere Fault.

Black star denotes one moderate size earthquake (ML: 4.5) recorded following the removal of the DANA array. Bottom and right inserts show projections of earthquake depths onto North-South and East-West profiles, respectively. Dashed red ellipses labelled *A, B, C* enclose regions of concentrated seismicity described further in the text. **b)** Earthquake depth histogram **c)** Earthquake magnitude histogram. We were able to precisely locate earthquakes with M_L magnitudes of 0.1.

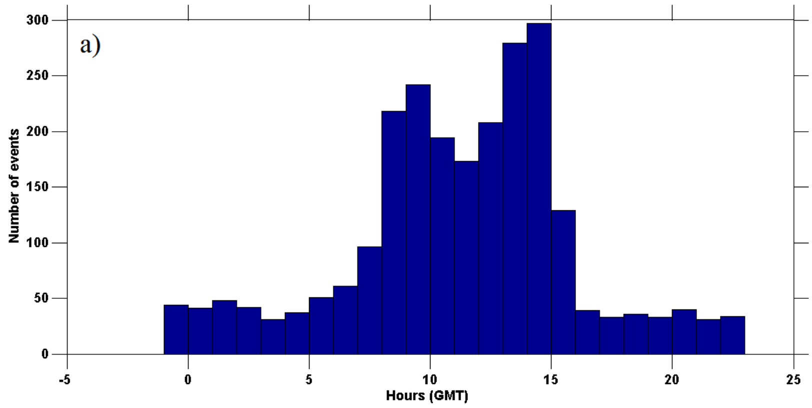

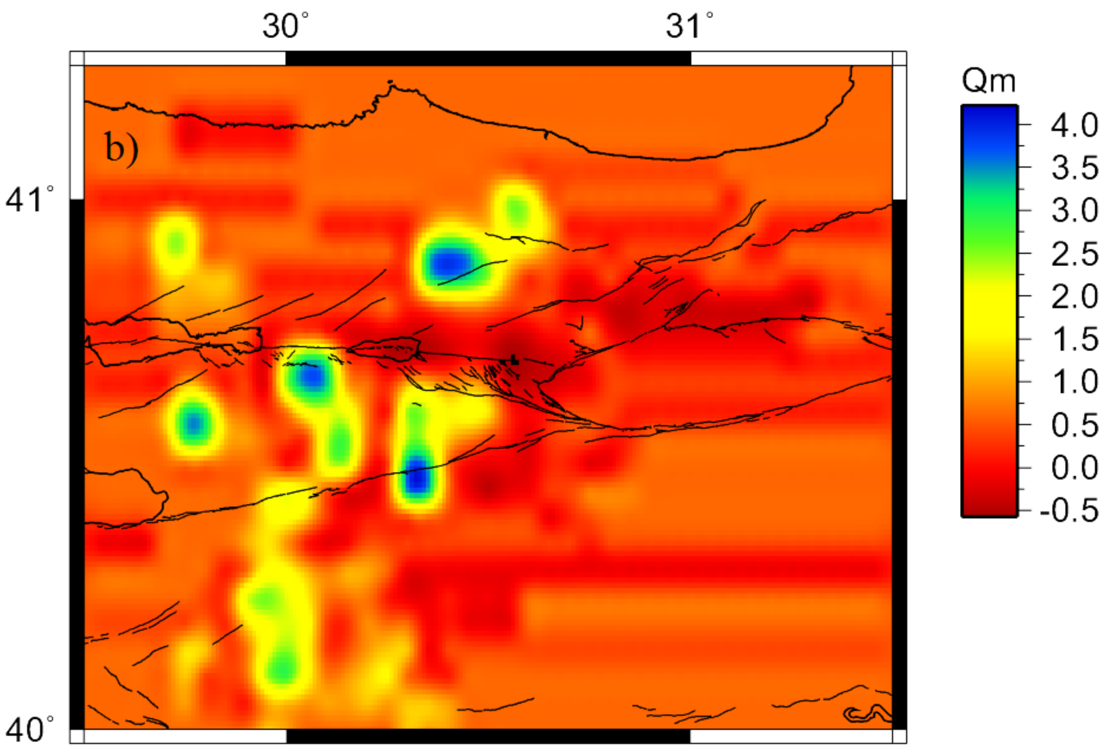

Figure 3: **a)** Event-time histogram. **b)** Map showing the Qm values for the study area. Darker green and blue colors (Qm > 2.5) indicate the presence of possible blast locations.

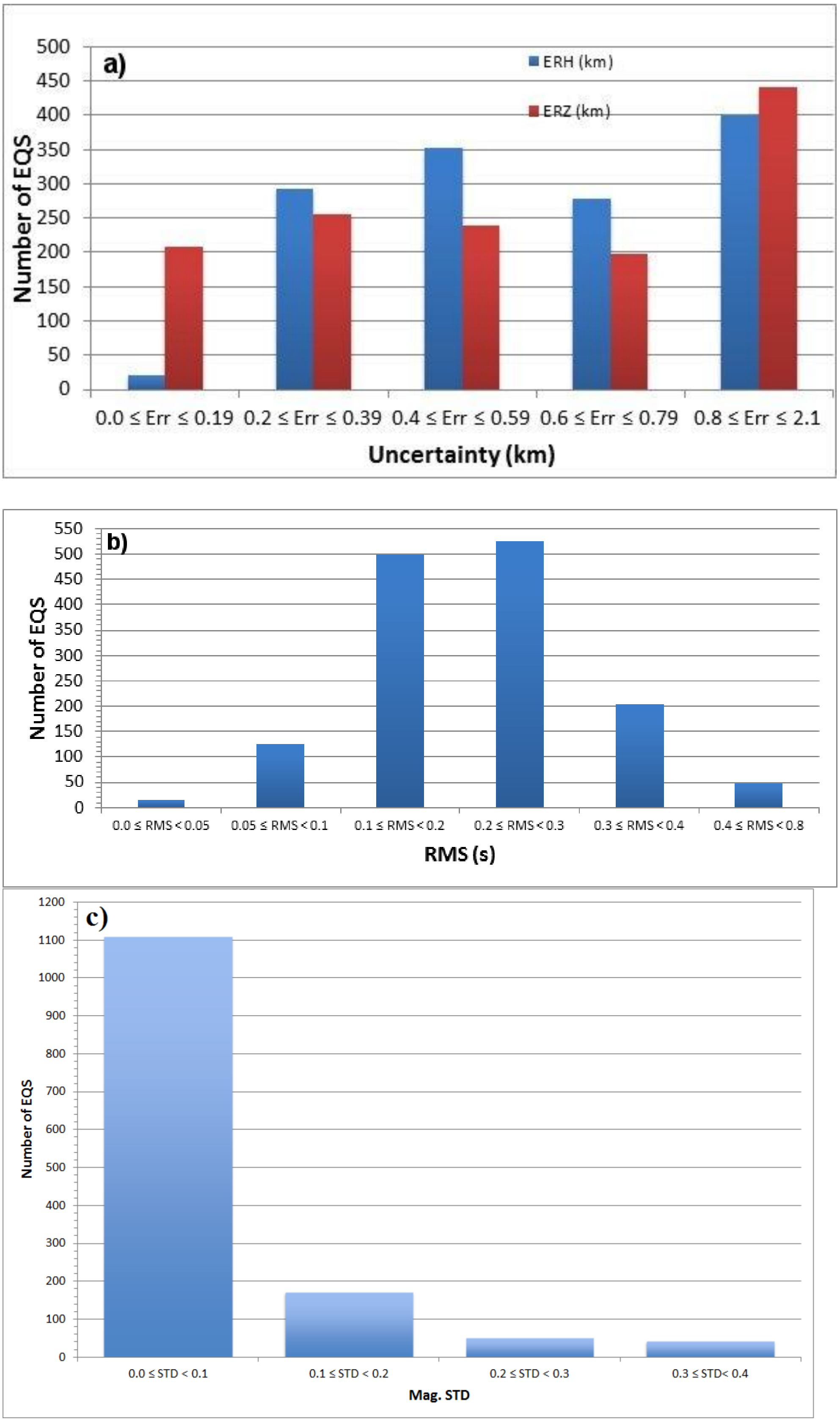

Figure 4: a) Histogram of horizontal and vertical location uncertainties. **b)** Histogram of RMS arrival- time misfits. **c)** Histogram of M_L standard deviation.

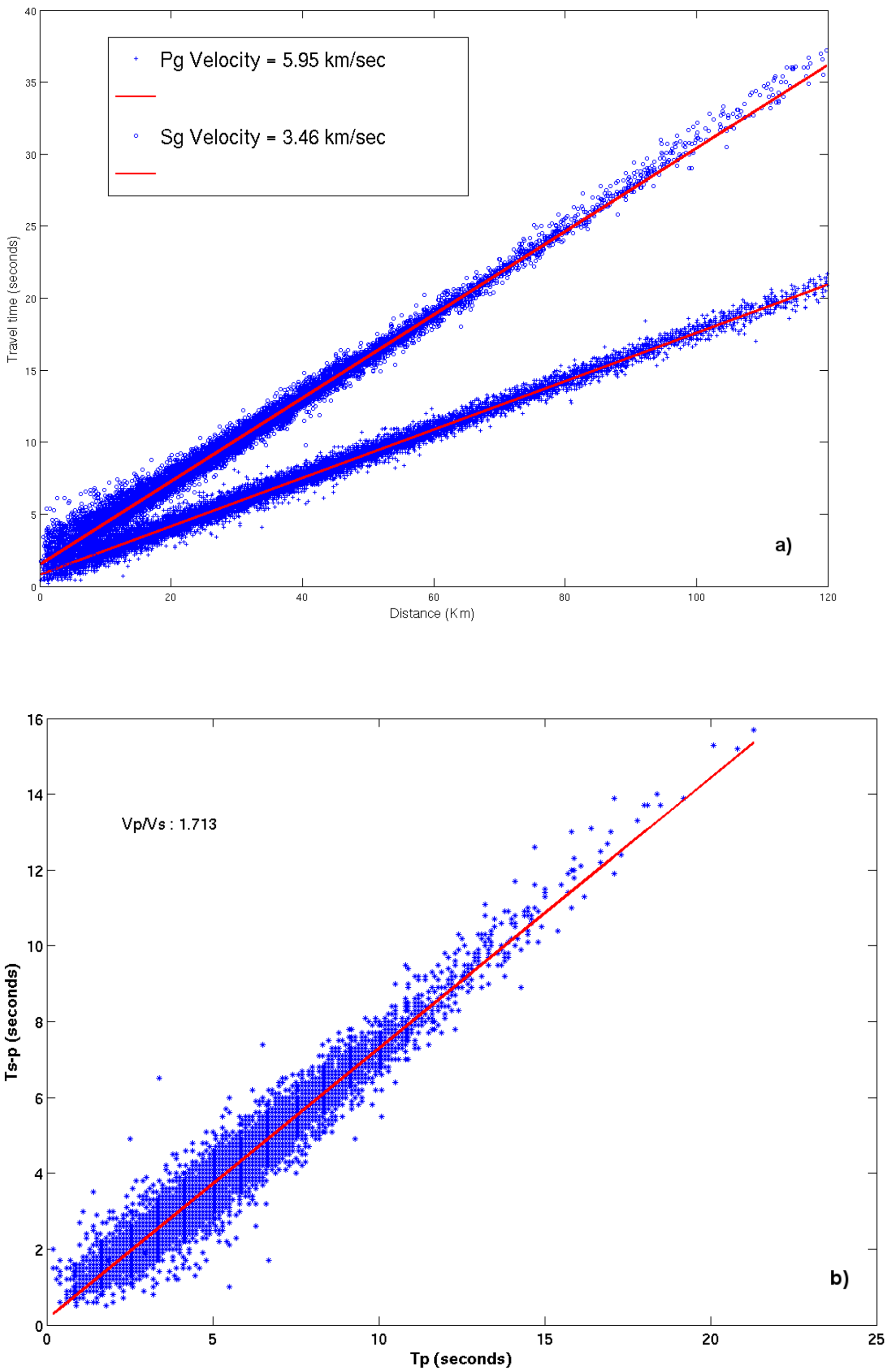

Figure 5: a) Travel times for Pg and Sg Phases. The best linear fit to the travel time data are shown by the red lines. **b)** Wadati diagram obtained using higher quality picks. Red line indicates the best linear fit corresponding to a Vp/Vs value of 1.713.

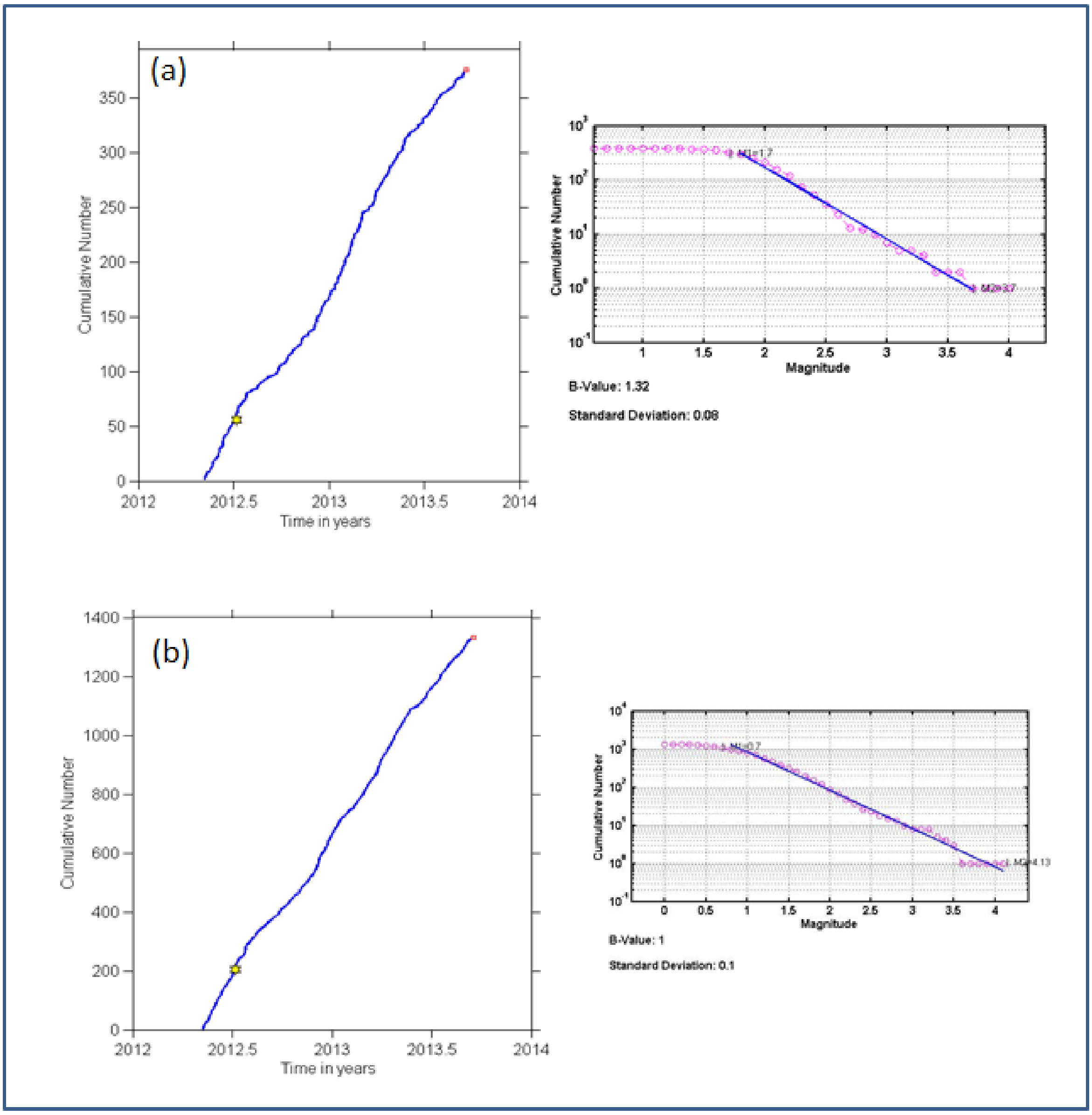

Figure 6: Comparison of cumulative number of earthquakes, M_c and the *b*-value found **a)** using the KOERI cataloque and **b)** using the DANA dataset. The Serdivan mainshock (M_L:4.1) is indicated by the yellow star. The existence of such a dense seismic network significantly decreased the Mc threshold and has permitted to a more accurate determination of the *b*-value.

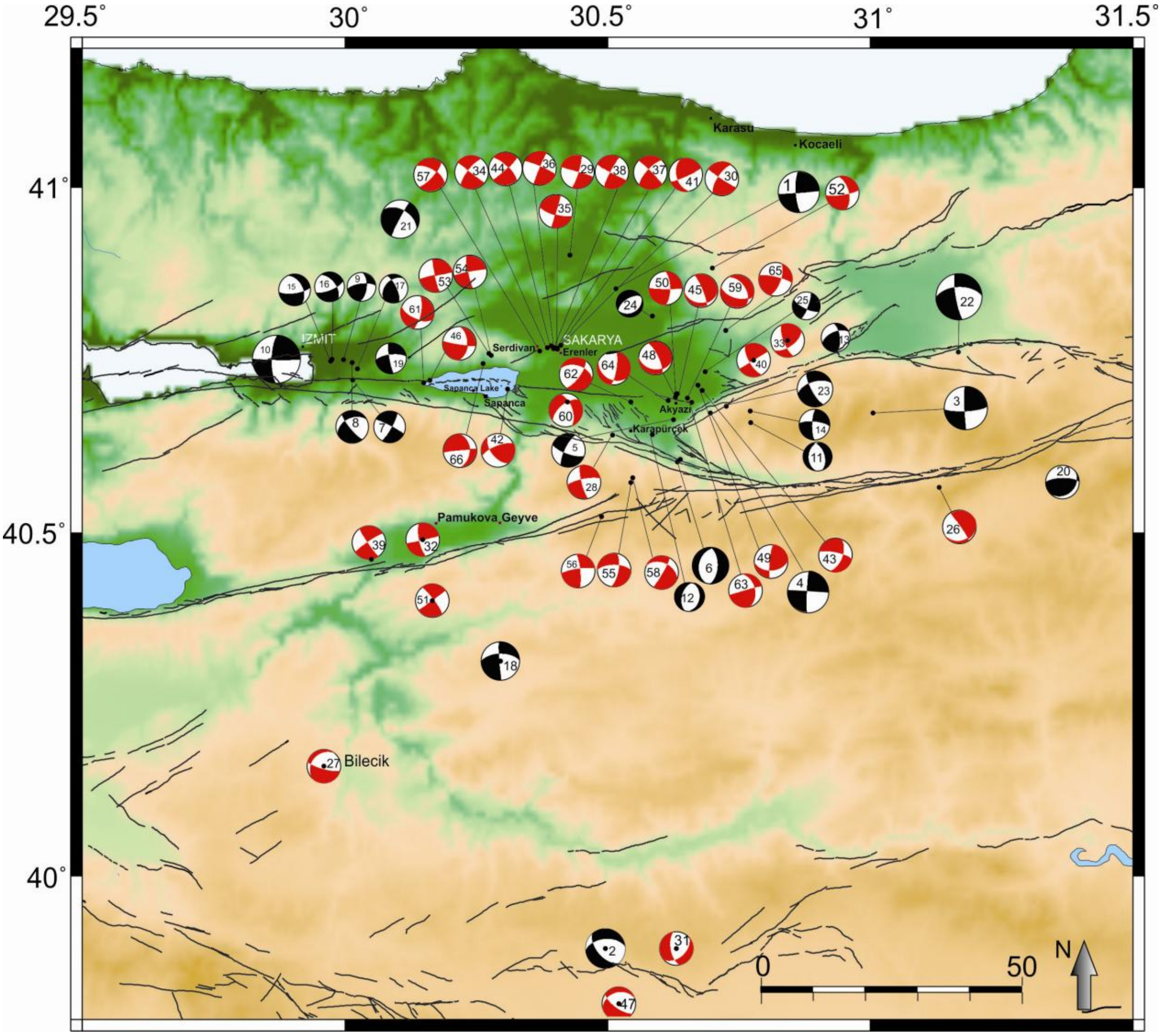

Figure 7: Focal mechanism solutions. Red beachballs show the 41 solutions from the current study and black beachballs indicate the solutions from various earlier studies listed in Table 2. Number 34 indicates the M_L: 4.1 Serdivan mainshock.

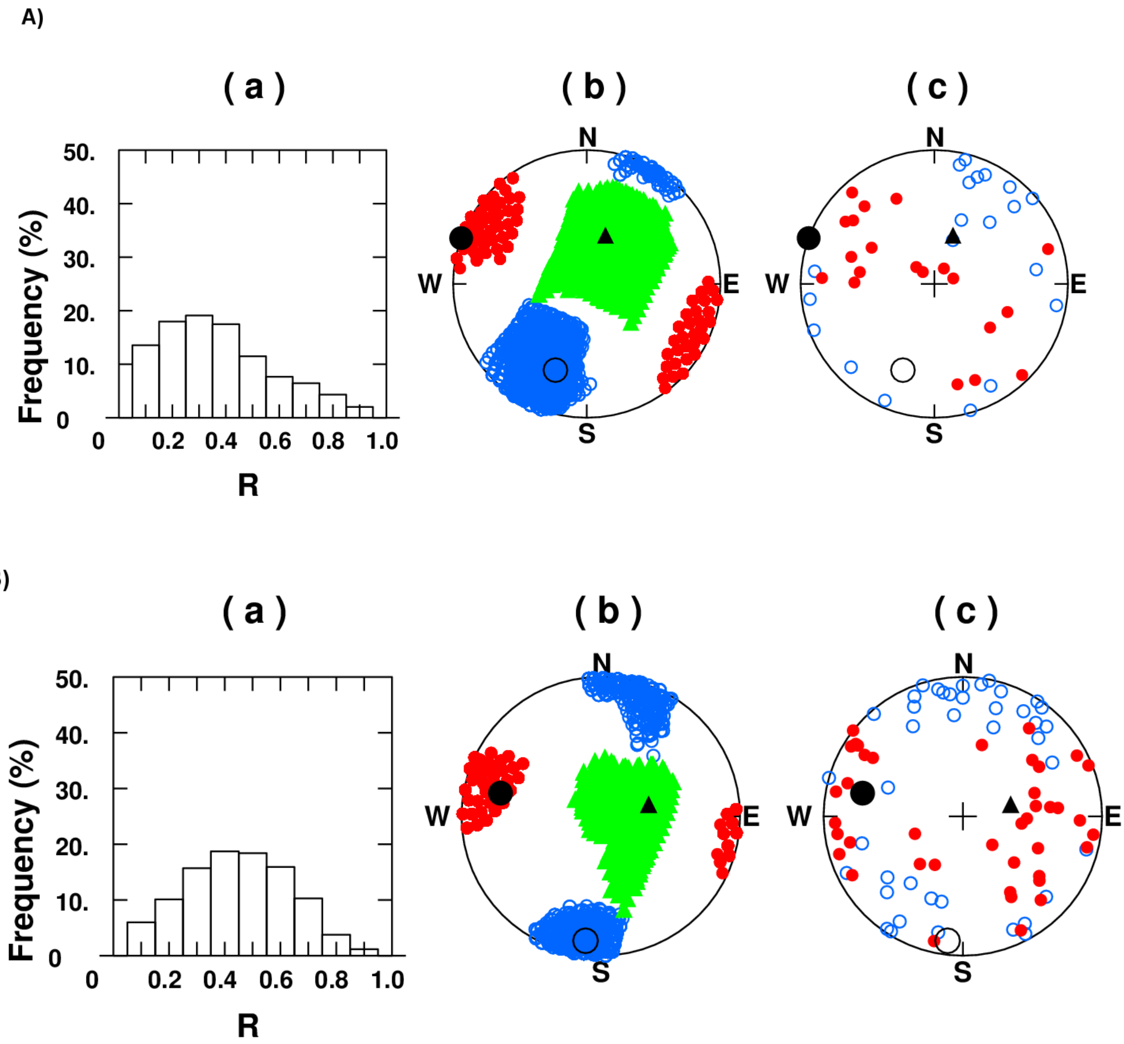

Figure 8: Stress tensor analysis from the P and T axes of the focal mechanisms. **A)** Analysis result for the 1999 İzmit Earthquake and its aftershocks, **B)** Analysis result for the M ≥ 1.8 earthquakes occurring within the operation period of DANA. Both panels show (a) the histogram of the R-value, (b) the distribution of the estimated principal stress axes and (c) the distribution of the observed P and T axes. In **(b),** red solid dots show the azimuth and plunge of the maximum compression axis σ_1, blue circles denote the minimum stress axis σ_3 and green triangles indicate the intermediate stress axis σ_2. In **(c),** red solid dots and blue circles show the P-axes and the T-axes, respectively. Black symbols denote the axes for the best fitting stress model.

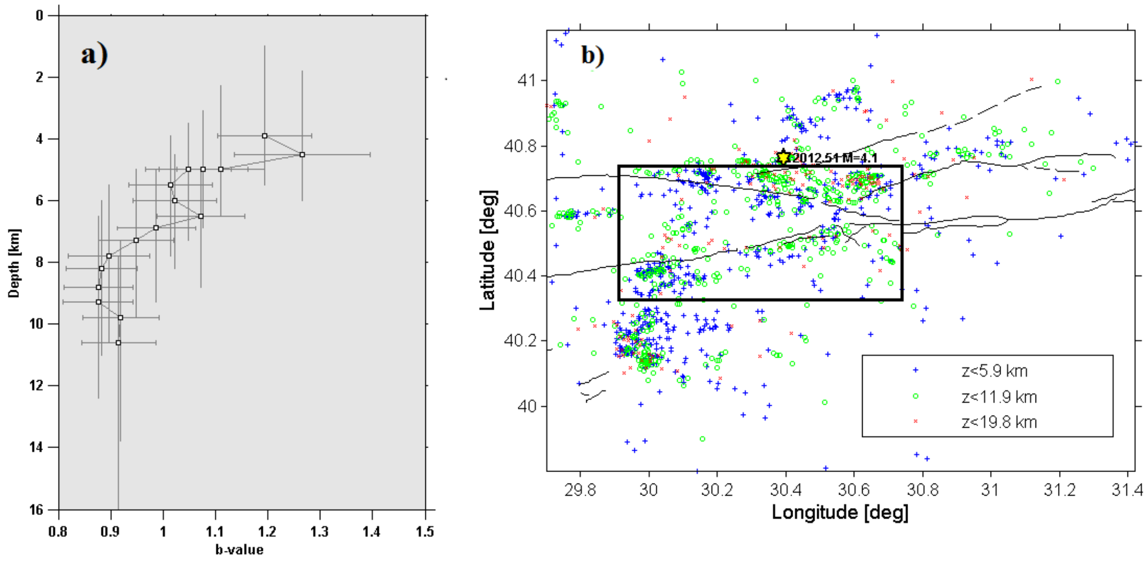

Figure 9: a) *b*-value variation with depth. Horizontal bars reflect the uncertainty in *b*- value estimations while vertical bars indicate the depth range sampled for the assigned window of 300 earthquakes. **b)** The selected area including the corresponding earthquakes. The colors indicate different depth (z) ranges.

S1

Click here to download Supplementary material for online publication only: Supplemantary1_earthquake_catalog.txt

S2

Click here to download Supplementary material for online publication only: S2.png

S3

Click here to download Supplementary material for online publication only: Supplemantary3_foreshockandaftershock.txt